Published in final edited form as:

Adv Mater. 2018 September ; 30(37): e1707634. doi:10.1002/adma.201707634.

Nanoscale Metal-Organic Frameworks for Therapeutic, Imaging, and Sensing Applications

Kuangda Lu[1,2], **Theint Aung**[1], **Nining Guo**[1,2], **Ralph Weichselbaum**[2], and **Wenbin Lin**[1]

[1]Department of Chemistry, The University of Chicago, Chicago, IL 60637, USA.

[2]Department of Radiation and Cellular Oncology and The Ludwig Center for Metastasis Research, The University of Chicago, Chicago, IL 60637, USA.

Abstract

Nanotechnology has played an important role in drug delivery and biomedical imaging over the past two decades. In particular, nanoscale metal-organic frameworks (nMOFs) are emerging as an important class of biomedically relevant nanomaterials due to their high porosity, multifunctionality, and biocompatibility. The high porosity of nMOFs allows for the encapsulation of exceptionally high payloads of therapeutic and/or imaging cargoes while the building blocks—both ligands and the secondary building units (SBUs)—can be utilized to load drugs and/or imaging agents via covalent attachment. The ligands and SBUs of nMOFs can also be functionalized for surface passivation or active targeting at overexpressed biomarkers. The metal ions or metal clusters on nMOFs also render them viable candidates as contrast agents for magnetic resonance imaging, computed tomography, or other imaging modalities. This review article summarizes recent progress on nMOF designs and their exploration in biomedical areas. First we discuss the therapeutic applications of nMOFs based on four distinct drug loading strategies, followed by a summary of nMOF designs for imaging and biosensing. We conclude our review by exploring the fundamental challenges facing nMOF-based therapeutic, imaging, and biosensing agents. We hope that this review can stimulate interdisciplinary research at the intersection of MOFs and biomedicine.

Keywords

Metal-organic framework; nanoparticle; nanomedicine; cancer therapy; imaging

1. Introduction

Metal-organic frameworks (MOFs), also called porous coordination polymers or porous coordination networks, are a class of crystalline hybrid materials constructed from metal ions or metal cluster nodes (also known as secondary building units, SBUs) and multitopic organic linkers. The regularity of coordination bonds enables isoreticular design of limitless MOF structures with high porosity and crystallinity. In the meanwhile, the relatively labile bonds between the ligands and the metal centers allow MOFs to be synthesized under mild conditions that are compatible with a number of organic functional groups. As a result, MOFs are distinct from the traditional inorganic materials with their molecular nature, versatile functionality, and structural and compositional tunability. Since early 1990s, MOFs

have garnered much attention for their potential applications in gas storage and separation,[1–6] nonlinear optics,[7, 8] ferroelectricity,[9, 10] conductivity/semiconductivity,[11–16] magnetism,[17] catalysis,[18–24] energy conversion,[25–27] luminescence and chemical sensing,[28–34] and other areas.[35–38]

The merging of nanotechnology and MOFs, in particular, has given rise to a new and promising material platform, nanoscale MOFs (nMOFs), with significant potential for biomedical applications. Compared to other nanoformulations, nMOFs present unique opportunities for biomedical applications due to three major structural attributes. First, the high porosity and large channels/pores of nMOFs are conducive to high cargo loading efficiency as well as facile transport of biomedical agents through nMOF channels. The latter merit is well recognized in the field of MOF catalysis but has been largely unexplored in biomedical areas up until recent years. Second, multiple functionalities can be readily and directly incorporated into nMOFs via appropriate selection and functionalization of the SBUs and organic linkers. This multifunctionality feature enables nMOFs to co-deliver and release drugs and/or imaging agents in a temporally and spatially controlled fashion, highlighting their potential roles as theranostic platforms and in synergistic combination therapies. Third, the tunable framework stability of nMOFs in physiological environments allows for the design of triggered or control release nanocarriers, which is difficult to achieve with other nanoformulations.

While Férey and coworkers studied the encapsulation of model drugs into and their release from bulk MOFs,[39] Lin and coworkers reported the first design of nMOFs as imaging agents in 2006.[40] Although MOF as a field has grown exponentially in the past decade, the use of nMOFs in biomedicine is mostly unexplored by the MOF community and largely under-appreciated by nanomedicine researchers.[41] The lack of appreciation for the potential of nMOFs in nanomedicine can be attributed to the unsatisfactory progress of current MOF research from a biomedical standpoint. Limited understanding of biology and medicine by most MOF researchers leads to a majority of research culminating in ‘proof-of-concept’ studies that are not clinically relevant. On the other hand, most biomedical researchers lack sufficient understanding of MOF chemistry to fully appreciate the potential of nMOFs in biomedicine. In this article, we will review the progress on biomedical aspects of nMOFs and highlight limitations of current works from clinical translation perspective. We hope that this review can also increase understanding and appreciation of nMOFs in the biomedical community and inspire interdisciplinary research activities at the intersection of MOFs and biomedicine to move this field forward.

2. nMOFs for Therapeutic Applications

The major aim of using nanoparticle formulations for drug delivery is to improve pharmacokinetics and alter the biodistribution of drugs, thus enhancing treatment efficacy and reducing side effects by preferentially accumulating drugs in diseased tissues. Specifically, nanoparticles can change the hydrophilicity of the drug, affect the pathway of drug uptake and efflux in tissues, and prevent drug molecules from non-specifically binding to bio-macromolecules. In oncological applications, nanoparticles of proper sizes and with suitable surface passivation have the propensity to passively target tumors by taking

advantage of the leaky vasculatures in tumors. In addition, tumors have defective lymphatic drainage, allowing for preferential accumulation of nanoparticles at the tumor sites. This combination of leaky vasculatures and defective lymphatic drainage in tumors is known as the Enhanced Permeability and Retention (EPR) effect. Furthermore, the surfaces of nanoparticles can be modified with biomolecule or small molecule ligands that selectively and avidly bind to the biomarkers overexpressed on cancer cells to further increase drug accumulation on tumors. It is expected that enhanced deposition of drugs on tumors will reduce systemic toxicity to other organs. In the co-delivery of multiple drugs with nanoformulations, the temporal release of these drugs can also be accurately controlled to maximize their synergistic effects.

A number of review articles have summarized the progress on drug delivery using nMOFs over the past few years.[37, 42] Instead of categorizing the works by the target therapies or drugs involved, we will focus on the strategies of incorporating therapeutics into nMOF delivery systems (Scheme 1). We will elaborate on the chemistry of each loading strategy and discuss the pros and cons for each of these approaches.

2.1 Encapsulation of Therapeutic Cargoes

Early research activities of the MOF community mostly focused on the storage and separation of different gaseous molecules by taking advantage of the high porosity and tunable pore and channels of MOFs. Naturally, non-covalent encapsulation became the most studied method of loading drugs to nMOFs. It was hypothesized that the nMOF channels will provide suitable accommodation for the typically hydrophobic therapeutic cargoes, preventing otherwise rapid clearance from the circulation and consequently, increasing drug accumulation in diseased tissues.

Horcajada *et al.* demonstrated the feasibility of noncovalent encapsulation of hydrophobic therapeutics into nMOFs in their pioneering work in 2006.[39] They tested the loading of ibuprofen (IBU) into two nMOFs, MIL-100 built from Cr^{3+} and trimesic acid with a BET surface area of 3340 m^2/g, and MIL-101 built from Cr^{3+} and terephthalic acid with a BET surface area of 5510 m^2/g. These nMOFs displayed remarkable drug loading capacities: 0.347 g IBU/g for MIL-100 and 1.376 g IBU/g for MIL-101. Further studies on the release kinetics of IBU suggested different types of interactions during drug encapsulation: relatively strong electrostatic interaction between the framework and cargo molecules, **π-π** interaction between hydrophobic drug and organic linkers, and weak hydrophobic interaction between the entrapped drugs. Noncovalent encapsulation is the most widely studied method for drug delivery due to its simplicity and use of operation.[37, 43, 44] Two stages of drug release —through free diffusion and upon nMOF decomposition— are expected for the encapsulated drug.

In their follow-up work in 2010, Horcajada *et al.* systematically studied drug delivery with a series of biocompatible Fe-nMOFs.[45] Several anticancer and antiviral drugs, including busulfan (BU), doxorubicin (DOX), azidothymidine triphosphate (AZT-TP), and cidofovir (CDV), were loaded into MIL-53, MIL-88A, MIL-88Bt, MIL-89, MIL-100 and MIL-101_NH_2 nMOFs with high encapsulation efficiencies and payloads. Drug release tests on AZT-TP, CDV, and DOX loaded MIL-100 in physiological conditions showed no burst

release, which is one major limitation of the non-covalent encapsulation strategy. The authors also evaluated the *in vivo* toxicity of nMOFs on rats. Observations for up to 3 months did not show significant differences between nMOFs and control groups on animal behaviors, body and organ weights, and serum parameters. Increase in liver and spleen weights was observed in the first week, but recovered to normal values at later times.

For charged frameworks, charge interaction can drive drug loading. Rosi and coworkers prepared an anionic network bio-MOF-1 with a formula of $Zn_8(ad)_4(BPDC)_6O•2Me_2NH_2•8DMF•11H_2O$ (ad refers to adenine).[46] The pillar-like SBUs can be described as $Zn_8(ad)_4$ octahedral cages bridged by Zn_4O clusters. In each $Zn_8(ad)_4$ unit, two pairs of Zn^{2+} from Zn_4O clusters take axial positions and coordinate with N3 and N9 positions of two adenines while the other four Zn^{2+} ions in the equatorial plane coordinate with N1 and N7 positions of the adenines. The zinc-adeninate columns are crosslinked by biphenyldicarboxylate linkers to form the **pcu** topology network. The framework has two negative charges per formula unit, balanced by ammonium counter ions. The authors showed that ammonium counter ions can be exchanged with cationic therapeutic agents such as procainamide,[46] or by lanthanide fluorophores, for near-infrared and visible light-emitting sensing.[47]

Several recent studies utilize “gatekeepers” to reduce the premature release of drugs to achieve targeted/triggered drug delivery. Tan *et al.* reported a proof-of-concept design of acid-responsive cap-protected nMOF drug delivery systems.[48] The authors attached pyridinium (Py) stalks to a Zn-based UMCM-1-NH_2 nMOF via post-synthetic modification, and loaded model drugs and carboxylatopillar[5]arene (CP5) caps. In neutral pH environments, the negatively charged CP5 can strongly interacts with positively charged Py moieties, functioning as a gatekeeper to prevent cargo release. In acidic environments, however, the protonated CP5 detaches from Py stalks and unblocks the pores. Although the acid-triggered switch properties were demonstrated, the system required low-pH conditions (pH=4 or below) and the vehicle itself was toxic. As a result, the *in vitro* and *in vivo* utility of this triggered nMOF delivery system was not adequately established. Nonetheless, follow-up works from these authors showed that similar capping strategies also responded to Zn^{2+} and Ca^{2+} concentrations in the cells, suggesting the generality of this design.[49, 50]

Wang *et al.* described a more complex modification strategy.[51] A MIL-101-N_3(Fe) nMOF with azide functionalities was modified with a bicyclononyne functionalized β-cyclodextrin derivative (β-CD-SS-BCN) through [3+2] azide-alkyne cycloaddition after doxorubicin (DOX) loading. An $\alpha_v\beta_3$ integrin targeting peptide functionalized polymer Lys(adamantane)-Arg-Gly-Asp-Ser-bi-PEG_{1900} [K(ad)RGDS-PEG_{1900}, where bi=benzoic imine] was further attached to the particle surface through host-guest interaction between the adamantyl group and β-CD (Figure 1a). The authors utilized two stimuli-responsive triggers in this smart design. The first trigger is achieved via the benzoic-imine bond between PEG and integrin targeting peptide that dissociates in acidic environment, leading to preferential accumulation of particles in tumors. The second trigger features the use of reducing agents such as glutathione in cancer cells to cleave the disulfide bond between β-CD and the nMOF to unblock the nMOF channels. A series of *in vitro* experiments indicated that cellular uptake of the nMOF system was pH and $\alpha_v\beta_3$ integrin expression-dependent whereas the

drug release was dependent on reductant concentrations (Figure 1b–d). *In vivo* efficacy studies by subcutaneous injection near the tumors (peritumoral injection) showed that DOX-loaded nMOF inhibited tumor progression as effectively as free DOX, but with fewer side effects (Figure 1e,f).

ZIF-8 built from zinc ions and 2-methylimidazolate provides an interesting nMOF for cargo encapsulation due to its relatively large pore cavities (11.6 Å in diameter) and narrow opening windows (3.4 Å in diameter).[52] As a consequence, while the pores are large enough to accommodate large drugs and biomolecules (usually a few angstroms to a few nanometers in size), the cargoes, once encapsulated inside the MOF during synthesis, cannot freely diffuse out through the small windows and can only be released upon nMOF decomposition.[52] Since ZIF-8 is stable in neutral aqueous environments and gradually decomposes in mild acidic conditions (pH≤6), it inherently functions as a pH-triggered release system (Figure 2). In the past few years, ZIF-8 has been used to encapsulate camptothecin (CPT),[53] doxorubicin,[54] proteins,[55–61] and inorganic particles.[62–64] This method is useful for delivery of large biomolecules and other cargoes that are larger than the pore size of nMOF.

Development of ZIF-8 nanocrystal growth methods under mild conditions enabled one-pot entrapment of cargoes into ZIF-8 during nMOF synthesis. Lai and coworkers reported a mild synthesis protocol for ZIF-8 nanocrystals in 2011.[65] Uniform nanocrystals with ~70 nm sizes can be synthesized by simply stirring a mixture of aqueous solutions of zinc nitrate and 2-methylimidazole at room temperature. Zhuang *et al.* reported the one-pot synthesis of cargo-loaded ZIF-8 nanoparticles using a similar method.[53]

Lyu *et al.* encapsulated the protein Cytochrome c (Cyt c) into ZIF-8 by polymer-assisted one-pot synthesis method.[55] The loading of Cyt c in the Cyt c/ZIF-8 composite was determined to be 8 wt% by ICP-MS. The conformation of Cyt c was retained after entrapment in ZIF-8 as indicated by steady-state fluorescence spectroscopy. Interestingly, the enzymatic activity of Cyt c/ZIF-8 was 10-fold higher than that of the free protein as indicated by hydrogen peroxide assay. The authors also prepared horseradish peroxidase/ZIF-8, lipase/ZIF-8 and Cyt c/ZIF-10 nanocomposites using the same method. This entrapment method is distinct from other works that immobilized small proteins/enzymes with MOFs.[66, 67]

Hill and coworkers demonstrated a rather different strategy for light-triggered drug delivery.[68] A thin layer of UiO-66 MOF was coated on an optical fiber. 5-Fluorouracil (5-FU) was then introduced into the MOF channels by sublimation. Drug release was triggered by 1050 nm light, the energy of which matches the binding energy of 5-FU to UiO-66 scaffold. This work introduced a new method to achieve light-triggered drug release.

2.2 Conjugations of therapeutic agents to the linkers

Therapeutic agents can also be readily attached to the ligands via orthogonal conjugation. Covalent attachment of the cargoes to the linkers can prevent premature release of cargoes while some conjugation strategies can introduce controllable triggers that disconnect upon certain chemical stimuli. A variety of chemical linkages, such as ester bonds,[69] amide

bonds,[70, 71] amine bonds,[72, 73] imine bonds,[74–77] urea formed from isocyanates,[71, 78, 79] thiourea formed from isothiocyanates,[79, 80] and click chemistry,[81, 82] have been employed to attach functional moieties to MOF linkers.

The cargoes can be conjugated to the organic linkers prior to the MOF growth or post-synthetically. Pre-functionalization of ligands ensures complete cargo loading and allows for thorough characterization of the drug conjugates. However, drug conjugation to the linkers lowers molecular symmetry and increases steric hindrance, thus impeding the growth and crystallographic characterization of MOFs. This approach is more often utilized to synthesize MOFs for other applications[83–85] than drug delivery due to the high molecular weights of most drug cargoes and stringent requirements of nMOF sizes and morphologies.[86] Post-synthetic modification, on the other hand, is widely used for drug conjugation due to the ease of operation and retention of particle morphology. However, the rigid structure of nMOFs limits or reduces accessible sites in the interior of the particles, rendering low conjugation efficiency in many cases. Post-synthetic attachment strategy is thus most suitable for surface modifications. Below we will showcase a few examples in which protection moieties or targeting groups are covalently conjugated to the nMOF surfaces whereas therapeutic agents are covalently attached to the linkers.

Lin and coworkers first demonstrated covalent conjugation of chemotherapeutic agents to the linkers in 2009 (Figure 3).[73] They incorporated amino groups to the framework by doping the terephthalic acid ligand with 2-aminoterephthalic acid during the growth of Fe(III)-MIL-101 nMOFs. A BODIPY dye (1,3,5,7-tetramethyl-4,4-difluoro-8-bromomethyl-4-bora-3a,4a-diaza-s-indacene, Br-BODIPY) and a cisplatin prodrug (ethoxysuccinato-cisplatin, ESCP) were conjugated to the ligands through amine and amide bonds, respectively. The particles were further coated with silica to retard the decomposition of the nMOF under biological conditions. The release half-lives of ESCP-conjugated nMOF with or without silica coating were 14 h and 1.2 h respectively, confirming the effective protection via surface modification. A silyl derived cyclic peptide targeting $\alpha_v\beta_3$ integrin was further attached to the particle surface and the nanocomposite showed comparable cytotoxicity to that of cisplatin on HT29 cells. This work demonstrated for the first time the possibility of covalently attaching cargoes to nMOFs for the delivery of both imaging and therapeutic agents to cancer cells *in vitro*.

Mirkin and coworkers reported the conjugation of DNA to UiO-66 nMOF surface via click chemistry.[87] Azide-functionalized UiO-66-N_3 nMOFs were synthesized from solvothermal reactions between 2-azidoterephthalic acid and $ZrOCl_2$. Dibenzylcyclooctyne (DBCO)-functionalized DNA was then reacted with the azido-nMOFs via Cu-free strained-alkyne click chemistry. The DNA conjugation decreased the particle ζ-potential and stabilized the particles in saline solution. Fluorescence quantification by flow cytometry showed a 6-fold increase of DNA uptake in HeLa cells after being conjugated to nMOFs.

Willner and coworkers recently extended this nucleic acid conjugation strategy to prepare ATP-responsive aptamer-based nMOFs for the controlled release of chemotherapeutics.[88] They loaded doxorubicin to the channels of Zr-amino-triphenyldicarboxylate nMOF that was previously reported by Lin and coworkers,[80, 89] and then capped the loaded nMOF by

hybridization with a complementary nucleic acid, the ATP-aptamer or the ATP-AS1411 hybrid aptamer, in caged configurations. The nMOFs are unlocked in the presence of ATP via the formation of ATP-aptamer complexes to release the drug payloads. Preliminary experiments with spheroid cell aggregates reveal the permeation of the ATP-AS1411-functionalized doxorubicin-loaded nMOFs into MDA-MB-231 breast cancer cells to afford high cytotoxicity. The *in vivo* targeting and efficacy of this aptamer-modified nMOF was however not demonstrated.

Lei and coworkers recently reported the design for an nMOF system for cancer imaging and chemo-photodynamic therapy.[90] They encapsulated camptothecin (CPT) into NH_2-MIL-101(Fe) nanocrystals and further modified the nMOF with Ce6-peptide and HOOC-PEG-Folate via amide bonds for cathepsin B (CaB)-triggered photosensitizer release and tumor-specific targeting, respectively. The final CPC@nMOF showed CaB-responsive fluorescence and photodynamic therapy (PDT) effect, as well as folate receptor-dependent cellular uptake. The authors then tracked *in vivo* fluorescence signal following injection with CPC@MOF, observing a gradually increase of tumor accumulation that peaked at 24 h. Although the covalent Ce6-peptide and HOOC-PEG-Folate conjugation to the nMOF was not fully elucidated, the *in vivo* Ce6 distribution by time-dependent fluorescence images supported this strategy of tumor-targeted drug delivery. In this regard, Lin and coworkers have established straightforward protocols to directly quantify the attachment of imaging and therapeutic agents to the linkers by NMR and mass spectrometry, which should provide a blueprint for future studies of conjugation of therapeutic agents to nMOF linkers.[80, 91]

Diring *et al.* reported a smart design of light-triggerable carbon monoxide (CO)-carrying nMOF.[92] UiO-67-type nMOFs built from Zr_6 clusters and 5,5'-dicarboxylate-2,2'-bipyridine ligands[93] were post-synthetically metalated with $MnBr(CO)_5$ via a controlled two-step loading method. Pre-metalation failed to work due to the decomposition of the Mn complex under nMOF growth conditions. The complex-loaded **CORF-1** nMOFs responded to 460 nm visible light to release CO based on the disappearance of CO stretching vibration peak by IR spectroscopy, while a $MnBr(dmbpy)(CO)_3$ molecular control failed to release CO due to aggregation-induced quenching between photoactive centers. Release studies indicated the complete (99%) release of CO in the **CORF-1** sample with 79% Mn complex loading, but lower release efficiency in the sample with 95% Mn loading. The authors proposed that the CO release was limited by light-penetration. White light-triggered CO release was also observed in Hela cells indicated by the lit-up fluorescence signal of a CO-responsive probe. This work thus demonstrated the feasibility of cargo loading via post-synthetic coordination of a metal complex.

Diring *et al.* also reported the use of pre-functionalized nMOFs for nitric oxide (NO) delivery.[86] Two nitroimidazole ligands, 2-nitroimidazole and 5-methyl-4-nitroimidazole, were employed to build zeolitic imidazolate frameworks of sodalite topology, namely NOF-1 and NOF-2. Upon Xenon lamp irradiation, NOF-1 and NOF-2 released 3.4 and 2.9 μmol/mg of NO, corresponding to conversion yields of 50% and 46% respectively. Interestingly, the light-induced NO generation of NOF-1 and NOF-2 was much greater than those of nitroimidazole ligands. The authors confirmed the light-induced NO release with two-photon confocal laser microscopy that has high spatial resolution. *In vitro* studies on

HEK293 cells genetically modified to express Transient Receptor Potential Channel 5 (TRPC5) protein showed that intracellular Ca^{2+} concentration rapidly responded to two-photon photoactivation of NOF-1. The pre-functionalization in this work nicely took advantage of the small cargo dimension and unique NO generation chemistry, but the amount of CO released from nMOFs was likely too small for therapeutic applications. MOFs containing diazeniumdiolate and bis-N-nitrosoamine moieties were also explored for NO release via post-synthetic nitrosation.[94, 95]

2.3 Therapeutic agents as linkers

Some therapeutically relevant agents can serve as linkers to build coordination polymers or MOFs. The direct incorporation of therapeutics as building blocks for MOF synthesis can circumvent problems with crystal growth often encountered when using pre-functionalized ligands. Such an approach also affords high atomic economy to lead to extremely high drug payloads. In this regard, several metal-peptide frameworks were constructed using simple oligopeptides such as Z-(L-Val)$_2$-L-Glu(OH)-OH as bridging ligands, but their potential biomedical applications have not been explored.[96–99]

A majority of drugs or prodrugs do not possess coordination geometry or molecular rigidity needed to construct crystalline MOFs, but they can be used to form amorphous nanoscale coordination polymer (NCPs). Since their first report of a NCP formed from lanthanide metal ions and a cisplatin prodrug in 2008,[100] Lin and coworkers have refined this strategy to prepare a series of surface-modified NCPs for chemotherapy, gene silencing, PDT, combined chemotherapy and PDT, and immunotherapy.[101–107] Significant progress has also been made to translate NCPs into clinic, but such amorphous nanoparticles are beyond the scope of this review.

If the therapeutic activity does not involve specific recognition or binding with biological targets, synthetic analogues with high symmetry and/or particular functional groups can be used as linkers for nMOF synthesis. Lin and coworkers were the first to successfully demonstrate the synthesis of nMOFs with porphyrin derivative-based linkers for PDT.[108] The DBP-Hf nMOF was constructed from 5,15-di(p-benzoato)porphyrin (H_2DBP) linkers and $Hf_{12}(\mu_3\text{-}O)_8(\mu_3\text{-}OH)_8(\mu_2\text{-}OH)_6$ SBUs and displayed a plate-like morphology (Figure 4).[109, 110] The as-synthesized nMOFs were shown to be highly stable in physiological media and efficiently generate singlet oxygen ($^1O_2$) upon red light irradiation while retaining their crystallinity. The authors also conducted *in vitro* cytotoxicity and *in vivo* efficacy studies on human head and neck cancer models to confirm the anticancer efficacy of nMOF-mediated PDT. In nMOF-treated group with 180 J/cm^2 light dose, two out of four mice had their tumors eradicated while the other two achieved 98% tumor regression. In comparison, the ligand control failed to inhibit the tumor growth at the same dose.

In addition to demonstrating the high efficacy of nMOF-based PDT, this work showed for the first time that structurally intact nMOFs could function at a molecular level *in vivo* by taking advantage of porous nMOF structures and small dimension of nMOF particles to afford a unique class of ideal nanophotosensitizers (nPSs).[111–116] In this nPS design, reactive oxygen species (ROS) including $^1O_2$ generated from nMOF-mediated PDT can readily diffuse out of the nMOF interior to exert cytotoxicity in cell milieu. Therapeutic

building blocks do not need to be released from nMOFs to fulfill their biological functions, which is a radical departure from traditional molecular nanocarriers whose primary purpose is cargo-trafficking and release following their disintegration upon delivery to target tissues.

Lin and coworkers further optimized the nMOF design by reducing the porphyrin ligand to its chlorin counterpart, 5,15-di(p-benzoato)chlorin (H_2DBC), and synthesized the first chlorin-based nMOF, DBC-Hf.[117] The DBC-Hf nMOF is isostructural to DBP-Hf, exhibiting a thin nanoplate morphology with thicknesses of 3.3–7.5 nm (Figure 4g). The lowest energy absorption of DBC-Hf red-shifted by 13 nm compared to DBP-Hf, providing improved light penetration through tissues. Furthermore, the extinction coefficient of DBC-Hf at the lowest energy Q-band increased by an order of magnitude when compared to that of DBP-Hf, improving its performance over DBP-Hf as an nPS for PDT. The authors demonstrated the superior PDT performance of DBC-Hf in *in vitro* and *in vivo* studies on two colon cancer models. DBC-Hf effectively regressed CT26 and MC38 tumors at low light and nMOF doses; in contrast, both H_2DBC ligand and DBP-Hf controls failed to inhibit tumor growth under identical conditions. By measuring calreticulin (CRT) expression on the surfaces of CT26 cells, nMOF-mediated PDT was also shown to induce immunogenic cell death (ICD), suggesting its possible role in priming the host immune system to enhance cancer immunotherapy.

Capitalizing on this finding, Lin and coworkers explored the combination of nMOF-enabled PDT with immunotherapy.[118] They synthesized another chlorin-based nMOF, TBC-Hf, comprising $Hf_6(\mu_3\text{-}O)_4(\mu_3\text{-}OH)_4(OH)_4(H_2O)_4(\text{carboxylate})_8$ SBUs and 5,10,15,20-tetra(p-benzoato)chlorin (H_4TBC) ligands (Figure 5). TBC-Hf nMOFs exhibited a nanorod morphology of 50–100 nm in length and 30–60 nm in width, possessing an identical structure to the previously reported MOF-545 which features large one-dimensional hexagonal channels. A small-molecule immunotherapy agent that inhibits indoleamine 2,3-dioxygenase (IDO) was non-covalently encapsulated into the channels of TBC-Hf with the hope that the IDO inhibitor (IDOi) could alter the immunosuppressive tumor microenvironment upon release from the nMOF and synergize with nMOF-mediated PDT to illicit systemic antitumor immunity. This hypothesis was confirmed by the abscopal effect observed on two bilateral syngeneic mouse tumor models of colorectal cancers. Both primary and secondary tumors regressed after IDOi@TBC-Hf injection and light irradiation to the primary tumor, indicating a systemic antitumor response induced by the combination therapy. This work thus established the potential of using nMOF treatment to enhance cancer immunotherapy for the first time. Future efforts are needed to elucidate the immunological mechanisms behind the interactions of nMOFs with the tumor microenvironment and immune cells in order to fully take advantage of nMOFs for cancer immunotherapy.[119]

Several other groups have followed up with more porphyrin-based nMOFs for PDT.[120] Liu and coworkers used a Hf-TCPP nMOF for combined PDT and radiotherapy.[121] Similar to the Zr-TCPP analogue previously reported by Zhou and coworkers,[122] the Hf-TCPP nMOF adopted PCN-224 structure with a diameter of 80–150 nm. PEG-grafted poly(maleicanhydride-alt-1-octadecene) (C18PMH-PEG) was used to coated the particle surface via hydrophobic interaction. The authors reported a single-compartment pharmacokinetics of the coated nMOFs by intravenous injection, with a blood circulation

half-life of 3.27 h. At 12 h post injection, ~7% injected dose of nMOF per gram of tumor was detected. Taking advantage of the high-Z metal Hf in the SBUs, the author suggested to combine radiotherapy and PDT to enhance the therapeutic effect. Since radiotherapy also consumes tissue oxygen which is required for PDT, the authors carried out PDT 8 h post radiotherapy. *In vivo* efficacy studies showed that combined radiotherapy and PDT more efficiently inhibited tumor growth than monotherapies.

Zhang and coworkers recently prepared a cancer cell membrane-camouflaged MOF nanocomposite that combines cell starvation therapy with nMOF-mediated PDT.[123] Glucose oxidase (GOx) and catalase were loaded on the surface of PCN-224. After loading, the particle size increased from 118.5 nm to 152.8 nm and the ζ-potential reversed from +24.5 mV to −10.3 mV. The particles were further coated by murine mammary carcinoma (4T1) cancer cell membrane fragments via extrusion method. The final nanocomposite mCGP had a hydrodynamic size of 227.5 nm and a ζ-potential of −20.9 mV. *In vivo* imaging study shows an efficient tumor accumulation of mCGP at 12 h post intravenous injection. Low fluorescence signals in livers and spleens suggested successful evasion of the particles from the mononuclear phagocytic system (MPS) although significant accumulation was detected in the lungs. *In vivo* anticancer efficacy study showed that mCGP more effectively suppressed the tumor growth than the dark control and single-enzyme (mCP and mGP with light) controls. While this work presents an intriguing approach toward nMOF surface modification, the uptake and interaction of these camouflaged nMOFs with the cells and any elicited immune responses need to be more closely examined.

2.4 Attachment of therapeutic agents to the SBUs

The metal-containing SBU is a unique feature of nMOFs compared to other nanoformulations. Although SBU coordination chemistry has been extensively studied in gas storage/separation and catalysis,[18, 124–126] SBU functionalization has only been explored for biomedicine in recent years. Some metal centers can directly function as therapeutic agents. For instance, Ag^{+}, Cu^{+}, Co^{2+} and Zn^{2+} ions are known for their potent antibacterial properties.[127] Hong and coworkers recently developed radioactive ^{89}Zr-based nMOFs for positron emission tomography (PET) and Cerenkov luminescence-excitable PDT.[128, 129]

Morris and coworkers explored nitric oxide storage and delivery with zeolites and MOFs using the metal-coordination strategy.[130, 131] NO coordinates to the metal centers in the Co-exchanged Zeolite-A or Cu centers in HKUST-1, affording high loading capacities of 1 mmol/g zeolite or 3 mmol/g MOF (room temperature, 1 bar), respectively. Rosseinsky and coworkers also used the SBUs to deliver NO.[132] Amine groups were incorporated via post-synthetic coordination of 4-(methylamino)pyridine (4-map) to the axial coordination sites on Cu centers in HKUST-1 nMOF with a 60% occupancy. The amino-functionalized nMOF was then exposed to 2 bar of NO to form N-diazeniumdiolate, resulting in the final composite with an empirical formula of $Cu_3(btc)_2(4\text{-map})_{1.8}(NO)_{0.7}$. The N-diazeniumdiolate formation was confirmed by the characteristic IR absorption bands. Proton transfer from the N-diazeniumdiolates to proximal amines was confirmed by ammonium cation N-H stretches in IR spectra.

Ma *et al.* coordinated carbon monoxide to the vacant metal sites in nMOFs for CO delivery.[133] MIL-88-Fe and NH_2-MIL-88B-Fe were activated in ultrahigh vacuum by removing terminal water before CO loading. The CO coordination mode was studied by FT-IR and Mössbauer spectroscopies. The release of CO in pH=7.4 phosphate buffer at 37 °C was monitored by a myoglobin assay. The release half-life was determined to be 38 min for MIL-88-Fe-CO and 76 min for NH_2-MIL-88B-Fe-CO, which are in good agreement with the degradation kinetics of these two nMOFs under the same condition.

Lin and coworkers delivered small interfering RNA (siRNA) using nMOFs by coordinating phosphate residues of nucleic acids to the SBU sites (Figure 6).[89] Plate-like nMOFs with a diameter of ~100 nm and thickness of ~30 nm were synthesized from $ZrCl_4$ and amino-triphenyldicarboxylic acid (amino-TPDC). A Pt(IV) prodrug and pooled MDR gene silencing siRNAs were sequentially loaded to the nMOFs via non-covalent encapsulation in the channels and phosphate coordination to the surface metal sites, respectively. The binding of siRNA to the nMOF surface effectively retarded the degradation of nucleic acid by RNase. The authors performed *in vitro* gene silencing and anticancer efficacy assays on a cisplatin-resistant ovarian cancer model to confirm efficient siRNA transfection and subsequent resensitization toward cisplatin drug treatment by the siRNA/nMOF nanocomposite. This work not only demonstrated siRNA delivery with nMOFs for the first time, but also shows that small molecular drugs and biologics can be co-delivered using multifunctional nMOFs to overcome drug resistance by cancer cells. Liu and coworkers used a similar strategy to prepare Se/Ru@MIL-101-siRNA nanocomposites for siRNA delivery.[134] Mirkin and coworkers attached DNAs to nMOF surfaces via phosphate coordination.[135]

Xie and coworkers loaded a boron-dipyrromethene (BODIPY) dye to the SBUs of nMOFs via carboxylate coordination.[136] Octahedral UiO-66 nanocrystals with a mean diameter of 70 nm were prepared by a solvothermal method, and carboxylate functionalized diiodo-BODIPY (I_2-BDP) was attached to the Zr_6 nodes via solvent-assisted ligand exchange. ICP-MS and UV-vis measurements gave an I_2-BDP loading of ~30wt%, whereas BET surface area and pore-size distribution analyses suggested that I_2-BDP was not encapsulated but bound to SBUs via ligand exchange. While the nMOF gave an increased cellular uptake of I_2-BDP, the *in vitro* PDT efficacies of free I_2-BDP and I_2-BDP-loaded nMOF were comparable, suggesting inhibited ROS generation and/or diffusion in the nMOF. Forgan and coworkers studied surface functionalization of UiO-66 nMOFs and *in vitro* drug delivery using PEGylated UiO-66.[137]

In some cases, biomolecules can be incorporated into the SBUs to build the frameworks. Tezcan and coworkers reported a series MOFs with SBUs based on ferritin, which is a globular protein complex consisting of 24 protein subunits.[138, 139] The authors mutated the amino acid position 122 of ferritin (originally threonine) to histidine, thereby creating a tripodal coordination motif near the C_3 symmetry pores for metal ion coordination. Through coordination with Zn(II), Ni(II) or Co (II), 8-connecting SBUs with cubic geometry were created and a library of ferritin-MOFs were constructed with precisely designed structures.

3. nMOFs for Imaging and Biosensing

The development of biomedical imaging technologies greatly facilitates the diagnosis of various diseases. Imaging agents can either produce signals or enhance signal contrast at targeted tissues. Nanoparticle imaging agents for cancer diagnosis preferentially accumulate in tumors via the EPR effect to achieve passive targeting or via tumor-specific receptor binding to achieve active targeting. In the past decade or so, nMOFs have been shown to be promising contrast agents for MRI, X-ray computed tomography (CT), and positron emission tomography (PET) by taking advantage of their metal connecting points or nodes. The incorporation of fluorophores to nMOFs has also enabled optical sensing and imaging of physiologically significant species. We will highlight the applications of nMOFs in bioimaging and biosensing applications in this section.

3.1 MRI

MRI is a medical imaging technique used to acquire high spatial resolution images of anatomy and physiological processes of the body. In its simplest form, MRI utilizes an external magnetic field, radio-waves and a gradient field to detect radio-frequency signals generated from protons, typically of hydrogen atoms in water from fat and tissues; the signals can then be used to contrast different tissues, distinguish lesions from healthy tissues and construct a map of anatomical structures in the body.[140] MRI contrast agents can alter longitudinal (T1) and transverse (T2) relaxation rates of water protons at the target tissue to generate image contrasts for diagnosis. Currently, the most commonly used T_1 contrast agents are gadolinium-based small molecules that have rather low sensitivity and occasionally cause nephrogenic systemic fibrosis on patients with severe renal impairment.[141] As linking multiple gadolinium complexes together has been shown to significantly increase r_1 relaxivity,[142] Gd-based nMOFs appear to be logical candidates as MRI contrast agents. On the other hand, the ability to encapsulate superparamagnetic nanoparticles in nMOFs allows for the design nanocomposites as T_2 contrast agents.[143]

Lin and co-workers first designed Gd^{3+}-containing nMOFs as MRI contrast agents in 2006.[144] Gd-BDC nanorods of ~100 nm in length and ~40 nm in diameter exhibited an r_1 relaxivity of 35.8 s^{-1} per mM Gd^{3+} or ~1.6 $\times 10^7$ $mM^{-1}s^{-1}$ on a per nMOF basis. This level of r_1 relaxivity is about an order of magnitude higher than that of Omniscan that is clinically used for MRI imaging of cancer and cardiovascular diseases. Interestingly, the nMOFs also exhibited a high r_2 relaxivity of 55.6 s^{-1} per mM Gd^{3+} or ~2.5×10^7 s^{-1} on a per mM of nMOF basis in an aqueous xanthan gum suspension. Two other novel Gd^{3+}-containing nMOFs with luminescent components were also reported by Lin's group as multimodal imaging probes for MRI and optical imaging.[145] However, potential leaching of toxic Gd^{3+} ions from nMOFs prevents further development of Gd^{3+}-containing nMOFs as MRI contrast agents.

To address the toxicity issue of Gd-based nMOFs, Lin and coworkers synthesized Mn-BDC and Mn-BTC nMOFs (BDC and BTC are to terephthalic acid and trimesic acid, respectively) as alternative MRI contrast agents because Mn^{2+} ions are known to be less toxic than Gd^{3+} and exhibit high r_1 relaxivities when bound to intracellular proteins *in vivo.*[146, 147] Mn-BDC nMOF exhibited r_1 and r_2 relaxivities of 5.5 and 80.0 $mM^{-1}s^{-1}$ on a per

Mn basis, respectively. The nMOF particles were further coated with a silica shell and tumor-targeting c(RGDfK) peptide to enhance uptake in HT-29 cells via receptor-mediated endocytosis. This work thus suggests the potential of constructing target-specific Mn-nMOF MRI contrast agents with low toxicity. Yang *et al.* synthesized Mn^{2+}-based nMOFs with near-infrared (NIR) dye (IR825) as organic linkers, which were shown to act as an MRI contrast agent and a photothermal therapeutic agent.[148]

Fe-based nMOFs have also been explored as potential MRI contrast agents. Horcajada *et al.* synthesized Fe-nMOFs for both MRI imaging and drug delivery.[45] Chowdhuri *et al.* synthesized nMOFs with Fe_3O_4 nanoparticles incorporated into their pores. These particles were further conjugated with chemotherapy drug paclitaxel and tumor-specific ligand folic acid, displaying strong T_2-weighted MRI contrast enhancement and a high drug loading capacity.[149] Other Fe-based nMOFs carrying chemotherapy drugs[150] or immunostimulatory oligonucleotides[151] have also been tested as MRI contrast agents.

3.2 X-ray Computed Tomography Imaging (CT)

CT imaging provides a powerful diagnostic tool for three-dimensional visualization of internal structures of a scanned object based on X-ray attenuation. In CT, X-ray is directed at an object at different orientations and a series of tomographic or cross-sectional images of the object are obtained at different beam paths, which are then used to reconstruct the volumetric presentation of the object.[152] Contrast agents with high X-ray attenuation such as iodinated aromatic molecules and barium sulfate are routinely used to provide contrast between targeted and adjacent tissues. However, due to nonspecific distribution, rapid clearance and extravasation from blood and lymphatic vessels, small molecular contrast agents currently used in the clinic are required at high doses, which induce adverse effects in some patients.[153] nMOFs have the potential to become CT contrast agents because high-Z elements can be easily incorporated into nMOF structures with extraordinarily high payloads.

Lin and co-workers developed UiO-66 nMOFs with high loadings of Zr (37 wt%) and Hf (57 wt%) and demonstrated their potential applications as CT contrast agents. Hf-nMOFs were coated with silica and poly(ethylene glycol) (PEG) to endow biocompatibility, and used for *in vivo* CT imaging of liver and spleen in mouse model.[154] Zhang *et al.* developed highly crystalline, monodisperse UiO-PDT nanocrystals via ligand exchange of photoactive iodine-BODIPY dyes in the UiO-type MOF framework. The nanocrystals were shown to not only have good biocompatibility and low toxicity, but also exhibit selective accumulation in tumor sites over adjacent tissues and organs in hepatoma-bearing rat models. Even at high injected doses at 100 mg kg^{-1}, there was no obvious severe acute or sub-acute toxicity.[155]

Gold nanoparticles have also been studied as contrast agents for CT imaging owing to the large X-ray absorption coefficient of gold. Shang *et al.* reported a gold nanorod-incorporated nMOF, Au@MIL-88(A), as a multimodal diagnostic agent to give high quality images in both MRI and CT imaging.[156] The gold nanorods were modified with 11-mercaptoundecanoic acid on the surface before being encapsulated into MIL-88(A) nMOFs. The nanocomposites display uniform star-like morphology with an average diameters of 89±3 nm, and have high contrast efficiency in CT imaging, T_2-weighted MRI, and

photoacoustic imaging.[156] The surface of nMOFs was modified with poly(ethylene glycol)-carboxyl acid (PEG-COOH) in order to protect MOFs from aggregation during the course of *in vivo* experiments. Both CT and MRI images acquired by using these particles as contrast agents show clear tumor boundaries with high penetration depth, spatial resolution, and contrast in subcutaneous and orthotopic human glioma models.

3.3 Optical imaging

Optical imaging (OI) utilizes light illumination to obtain images of organs, tissues and cells based on the detection of ballistic or diffusive photons. It is minimally invasive to the patients and is highly sensitive but the shallow penetration of light limits its use in the clinic. Near-infrared dyes offer a greater penetration depth, but near-infrared OI is still limited to shallow depth of < 1 cm. Foucault-Collet *et al.* synthesized near-infrared–emitting nMOFs, incorporating a high density of Yb^{3+} lanthanide cations and phenylene-derived photosensitizers.[157] Yb^{3+}-based nMOFs were endocytosed by cells and retained in cytosol, emitting a sufficiently high number of photons per unit volume to enable live imaging of HeLa and NIH 3T3 cells despite the relatively low photoluminescence quantum yield.

OI is compatible with and complementary to other imaging and therapeutic modalities. Li *et al.* developed core-shell nanocomposites for luminescent/magnetic dual-mode imaging.[158] Yb- and Er-doped $NaYF_4$ upconversion nanoparticles (UCNPs) were surface-modified with polyvinylpyrrolidone (PVP) before *in situ* growth of Fe-MIL-101-NH_2 shell on the particle surface. The UCNP@MOF nanocomposites with average diameters of ~120 nm were further modified with PEG and PEG-folic acid (FA) to increase biocompatibility and incorporate targeting functionalities. *In vitro* studies confirmed that FA-targeted nanocomposites can be selectively uptaken by the folate receptor overexpressed KB cells. *In vivo* optical imaging and T_2-weighted MRI studies also showed significant KB tumor contrast at 24 h post intravenous injection (Figure 7). Cai *et al.* developed MIL-100 (Fe) nMOFs with hyaluronic acid (HA) surface coating for targeting. They also loaded the nMOFs with a NIR dye, indocyanine green (ICG), for image-guided photothermal cancer therapy.[159] This particle showed a high loading content of ICG (40 wt%), strong NIR absorbance, and photostability. The *in vitro* and *in vivo* imaging studies demonstrated that MOF@HA@ICG NPs showed high cellular uptake in CD44-positive MCF-7 cells and enhanced accumulation in xenograft tumors due to their targeting capability.[158–160]

3.4 Positron Emission Tomography

PET is a nuclear functional imaging technique that enables visualization of metabolic processes in the body. In PET, positron-emitting radionuclides accumulating at the target organs generate pairs of gamma ray photons that can be captured by sensitive detector panels. A dedicated software is used to triangulate the source of emissions, creating 3D computed tomography images of radionuclide concentrations within the body. Compared with other imaging techniques, PET imaging has superior detection sensitivity, deeper signal penetration, and better quantitation capability.

Hong and coworkers reported a proof-of-concept design of ^{89}Zr-containing nMOF for PET imaging (Figure 8).[128] The radionuclide ^{89}Zr was incorporated into the SBUs of UiO-66

nMOFs, and the nanoparticles were further functionalized with pyrene-derived PEG and conjugated with a tumor-targeting peptide ligand (KDEPQRRSARLSAKPAPPKPEPKPKKAPAKK, F3). The *in vivo* organ distribution of ^{89}Zr-UiO-66/Py−PGA-PEG-F3 nanoparticles was traced by PET scans and an 8.2±0.3% total injected dose/gram of tumor was detected at 2 h post intravenous injection. On the other hand, it was shown that the non-targeted particles and F3-blocked groups gave 3–4 folds lower tumor accumulation doses at the same time point. However, significant particle accumulations were also seen in the livers and spleens, suggesting non-specific uptake by the MPS. Nonetheless, ^{89}Zr-based nMOFs provide as a potential option for PET imaging. Given that the half-life of ^{89}Zr (78h) is much longer than that of traditionally used ^{18}F (~2 h), Zr-MOF PET agents can potentially be designed for relatively long-term imaging.

3.5 Biosensing

The development of molecular sensors to probe physiological processes is a burgeoning research area. Disruptions or pathological changes in physiological environments can result in changes in the concentrations and types of metabolites in cells. The ability to detect and monitor these changes with specific and sensitive sensors will help diagnose diseases and reveal the underlying biology. nMOF-based sensors overcome the self-quenching and leaching problems of many small-molecular biosensors to achieve high sensitivity, resolution, and precision in subcellular biosensing. The ability to attach multiple functionalities to nMOFs allows for the design of multi-target, ratiometric, or Förster resonance energy transfer (FRET) sensors. Several studies have appeared in the literature with different nMOF-based sensors tested in cellular and subcellular sensing.

Intracellular pH plays an important role in physiological environments, regulating cellular functions and physiological activities. The pH dysregulation in intracellular fluids is related to tumorigenesis and drug-resistance.[161] Real-time sensing and monitoring of pH changes inside live cells are therefore important for probing disease mechanisms and designing pH-responsive intracellular drug delivery systems. Lin and coworkers reported the first nMOFs for real-time intracellular pH sensing.[80] Fluorescein moieties were attached to the Zr-based UiO nMOFs through thiourea bonds. The relative fluorescence intensity associated to two excitation wavelengths (435 nm vs 488 nm) changes with pH, which allows for ratiometric determination of environmental pH. Taking advantage of the preferential endocytic uptake of the nanoparticles, live cell confocal microscopy imaging was performed to illustrate the acidification process during endosome maturation with high spatial resolution and fast temporal response. This study also offered new insights into the processes of endocytosis and intracellular trafficking of nMOFs.

Various diseases such as cancer or vascular diseases can induce hypoxia, a reduction of oxygen level in the tissue. Common cancer treatment modalities such as radiation therapy, chemotherapy, and PDT are all highly oxygen-dependent and therefore, intracellular oxygen sensing is important for cancer diagnosis and therapy. Lin and coworkers designed the first phosphorescence/fluorescence dual-emissive nMOF for ratiometric intracellular oxygen quantification (Figure 9).[91] The mix-ligand M-nMOF containing an oxygen-responsive phosphorescent ligand, Pt-5,15-di(p-benzoato)porphyrin, and an amino-functionalized

ligand, amino-quaterphenyldicarboxylate, was first synthesized. Rhodamine B was then covalently attached to the amino groups via thiourea bonds as an oxygen-independent reference to afford R-nMOF. The two chromophores shared the same excitation energy while the phosphorescence/fluorescence emissions did not interfere each other. The ratiometric photoluminescence method for oxygen quantification was then established, allowing for the determination of oxygen levels in hypoxia, normoxia or aerated cells by live-cell confocal microscopic imaging with the R-nMOF.

Many gaseous molecules, such as nitric oxide and hydrogen sulfide (H_2S), constitute an important class of biological molecules involved in cellular metabolism. Wu *et al.* developed Cu^{2+}-based nMOF with triphenylamine emitters which are highly sensitive to NO concentrations in living cells.[162] The reduction of Cu(II) in the SBUs to Cu(I) by NO can prevent ligand luminescence quenching by paramagnetic Cu(II) centers to turn on the fluorescence signal. This nMOF sensor displayed moderate sensitivity but excellent selectivity to NO. Tang and coworkers designed a PAC nMOF for H_2S sensing.[163] The Cu-porphyrin containing nMOFs lose the Cu(II) coordination upon H_2S exposure, which turns on the porphyrin fluorescence. This H_2S probe selectively respond to H_2S and can detect as low as a few tens of micromolar H_2S in live cells. Several nMOF sensors base on metal-sulfide formation or reduction of organic functional groups have also been reported in recent years.[164–166]

Metal ions are another important class of physiologically important species. Several metal ions play key roles in cellular activities but their presence in high concentrations can be toxic and lethal. It is thus important to selectively detect metal ions in cells for diagnosis purposes. To this end, MOFs provide a platform for designing fluorescence turn-off sensors since energy/charge transfer between the ligands and the metal ions can lead to fluorescence quenching. Lu *et al.* developed nMOF-253 with 2,2'-bipyridine-5,5'-dicarboxylic acid (bpydc) ligands for Fe^{2+} detection.[167] The ligand fluorescence was selectively quenched by Fe^{2+} likely due to photo-induced electron transfer, allowing for the nMOF to be used for intracellular Fe^{2+} sensing in HeLa cells. nMOF-based systems to detect metal ions such Cu^{2+} and Fe^{3+} have been developed based on luminescence quenching of the Tb^{3+} or Eu^{3+} ions.[168, 169] Water stable MIL-53(Al) and Zr(IV) based BUT MOFs have also been reported as Fe^{3+} sensors, based on SBU ion exchange and Lewis base-induced ion inclusion in the channels, respectively.[170, 171]

Nucleic acid is at the center of physiological regulation. Detection of DNAs and RNAs is important for diagnosis of many diseases and biological processes, including cancer or other cell dysfunctions, drug resistance, and immune responses.[172] Several nMOF-based nucleic acid sensors have emerged in recent years, most of them using fluorescence quenching by binding nMOFs to DNA detectors as signal readout.[173–177] For example, Chen and coworkers absorbed a triplex-forming oligonucleotide on a H_2dtoaCu nMOF to recognize double-strand DNA, reaching a detection limit of 1.3 nmol/L towards HIV DNA with good selectivity. Huskens and coworkers recently reported another strategy by covalently and non-covalently modifying the MIL-88A nMOF via "click" chemistry.[178] Biotin moiety was first covalently conjugated to the MOF surface, then peptide nucleic acid (PNA)-conjugated biotin was attached by non-covalent interaction between biotin and Alexa-Fluor488-labeled

streptavidin. The PNA-functionalized nMOFs selectively bound to DNA to differentiate among fully complementary, single-base mismatched, and randomized DNA targets in cells by flow cytometry and confocal microscopy.

Zhao *et al.* developed a near-infrared luminescent nMOF as a highly sensitive self-calibrated thermometer in the physiological range.[179] This LnMOF composed of 1,3,5-benzenetrisbenzoic acid displayed excellent temperature-dependent photoluminescence properties within the physiological window from 303 to 333 K, and showed a maximum relative sensitivity of 4.8% K^{-1}. With the temperature resolution at 0.01 K, these nMOF sensors can detect temperature differences between pathological cells and normal cells.

4. Fundamental Challenges and Outlook

We have discussed the design of nMOFs for potential applications in therapy, biomedical imaging, and biosensing in previous sections. Here we focus on the fundamental challenges facing nMOF-based therapeutic, imaging, and biosensing agents. We will divide discussion into three areas: controlled synthesis, biodistribution, and biocompatibility/toxicity.

4.1 Preparation: size control and surface modification

Although tens of thousands of MOFs have been synthesized in the past twenty years, few of them were specifically designed for intended applications.[36, 37, 180] Many methods have been utilized to synthesize MOFs, including solvothermal/hydrothermal, electrochemical, mechanochemical, sonochemical, and continuous flow methods. Solvothermal synthesis is by far the most commonly used method for nMOF growth owing to its versatility and applicability toward a wide variety of MOFs. A number of alternative strategies have also been adopted to prepare nMOFs of diverse compositions.

Lin and coworkers developed surfactant-assisted microemulsion method for nMOF synthesis.[40] Through a precise control of water-to-surfactant ratio (W-value) as well as the pH of the reaction and substrate concentrations, the particle sizes can be closely controlled. Maspoch and coworkers used a spray-drying method to prepare various types of nMOFs.[181] Kundu et al. downsized a Gd(III)-based MOF to the nanoscale via a mechanical grinding method, but the generality of this approach was not demonstrated.[182] However, reaction parameters have not been systematically optimized for the synthesis of most nMOFs and there is no clear rule for predicting or controlling the sizes and morphologies of nMOFs. A number of conditions have to be screened on a trial and error basis. The reproducibility of nMOF synthesis is another issue due to the complexity of the parameter space.

Particle size is another important parameter that dictates biological fates and functions of nMOFs as particle size strongly affects the biodistribution of systemically administered nMOF particles.[183] It is now established that particles smaller than 6 nm are rapidly eliminated via renal filtration while those larger than 200 nm accumulate in liver and spleen via rapid MPS clearance.[184, 185] The size and shape of particles can also influence the cellular uptake as reported in several studies.[122, 186, 187] Hydrodynamic sizes of nMOFs should thus be carefully controlled to optimize their in vivo performances.

Surface modification controls particle stability, cellular uptake, and particle opsonization through protein adsorption. Silica coating on nMOFs is particularly useful for stabilizing physiologically unstable nMOFs, increasing biocompatibility, and allowing further functionalization with silyl-derived molecules. Lin and coworkers have developed a series of nMOF formulations with silica coating via polymer-assisted tetraethylorthosilicate treatment or direct sodium silicate treatment.[73, 146, 188]

Polymers are also widely used for nMOF surface modification. PEG and its derivatives are most commonly used to prevent MPS clearance. Typically, PEG moieties are incorporated onto MOF surfaces via non-covalent interaction,[121] or conjugated to the organic linkers[158] or the SBUs.[137] Other non-PEG-based polymers such as cyclodextrin, [51, 189, 190] heparin,[191] hyaluronic acid,[159] and other biocompatible polymer[192, 193] are also used to modify nMOF surfaces.

Over the past few years, nMOFs have also been coated with nucleic acids via both covalent attachment and non-covalent interactions.[87, 89, 134, 135] Zhang and coworkers recently reported cancer cell membrane-camouflaged nMOF nanocomposites to evade the MPS, but this coating increased particle size, thereby causing lung accumulation.[123] In addition, nMOFs have also been modified with various targeting moieties such as folates,[158] integrin-targeting peptides,[51, 73] and aptamers,[88, 194] to increase their uptake in cancer cells. Despite significance progress in surface modifications and active targeting of nMOFs, accurate characterization of coating/targeting efficiency and stability is still an unsolved challenge. Rigorous *in vitro* and *in vivo* studies are needed to realize the full potential of nMOF-based imaging and therapeutic agents.

4.2 Biodistribution of nMOFs

The main goal of nanoparticle delivery is to improve the pharmacokinetics (PK) of therapeutic and/or imaging agents. The particle size, shape, surface chemistry, and colloidal stability greatly affect the trafficking, clearance, and tumor uptake of nanoparticles.[195] For nMOFs, their intrinsic crystallinity and rigidity often lead to very well-defined shapes (cubes, rods, discs, etc.) for which the sizes are more difficult to be controlled than for conventional nanocarriers that tend to be spherical. Surface passivation methods are also less developed for nMOFs than for conventional nanocarriers that have been refined over the past four decades. Consequently, few nMOF formulations display biodistribution profiles that are comparable to those of well-characterized nanocarriers such as liposomes.

Early studies of nMOF drug delivery did not routinely report their biodistributions. Many recent nMOF delivery studies have examined the pharmacokinetics and biodistribution of therapeutic cargoes *in vivo*. Li *et al.* reported the biodistribution of nMOFs in tumor bearing mice 24 h post injection using ICP-MS.[158] Liu and coworkers monitored the blood concentrations of nMOFs via ligand fluorescence and reported mono-component PK of nMOFs in their recent work.[121] Zhang *et al.* and Cai et al used *ex vivo* fluorescence imaging method to track the biodistribution of their nMOF formulations.[123, 159] This method can be influenced by the differences in organ sizes, limited penetration depth of light, scattering of photons, and non-uniform fluorophore localization in each organ, and thus cannot be considered a quantitative method. Hong and coworkers reported the PK of

their nMOF particles and showed that suboptimal particle sizes caused rapid MPS clearance and undesirable biodistribution.[128]

As PK and biodistribution play an important role on the performance of any nanocarrier, we expect that more effort will be devoted to elucidating the fate of nMOFs after systemic administration. For systemically administered nMOFs, only after achieving favorable PK and biodistribution can we expect their successful translation to the clinic. On the other hand, as demonstrated by Lin and coworkers,[118] intratumoral nMOF administration plus light irradiation can be used in combination with checkpoint blockade immunotherapy to achieve systemic tumor regression via abscopal effects, indicating that rationally designed nMOFs can have clinical value even if they require local injection.

4.3 Biocompatibility/Toxicity

The toxicity and long-term effects of nMOFs have not been thoroughly characterized in most published studies. The accumulation of biocompatibility/toxicity data on nMOFs will be a key factor for facilitating the translation of nMOFs into clinical practices. Limited published data on nMOF toxicity already provided some guidance on designing nMOFs for clinical translation. Horcajada and coworkers analyzed the toxicity of three Fe-based nMOFs *in vivo* and observed that the particles were quickly uptaken by the major RES organs following intravenous injection, as is typical for large and surface un-passivated nanoparticles.[196] After gradual degradation of nMOFs, the polycarboxylate linkers were detected in the urine and feces samples; however, they noted that the temporary iron overload caused reversible oxidative stress in livers and spleens that recovered only after the removal of excess iron by excretion.

In a large scale study, Masposh and coworkers systematically characterized the culture medium stability and toxicity of a library of nMOFs including MIL-100, MIL-101, HKUST-1, NOTT-100, ZIF-7, ZIF-8, MOF-74 family, UiO-66, UiO-66-NH_2, UiO-67, and MOF-5.[197] The decomposition of uncoated nMOFs upon cell culture medium incubation at 37 °C was analyzed by powder X-ray diffraction and ICP-OES quantification of metals in the solutions. UiO-66, UiO-67, MIL-100, MIL-101, and ZIF-7 were mostly stable after 24-h incubation; ZIF-8 and a few MOF-74 nMOFs slightly degraded but retained their crystallinity; MOF-5, HKUST-1, NOTT-100 and most of MOF-74 nMOFs lost their crystallinity upon incubation (Table 1). The toxicity of the nMOFs were tested by *in vitro* XTT assay and *in vivo* zebrafish embryo assay (Table 1). The authors found that nMOF toxicity is strongly correlated to the metal toxicity. Other factors such as new species formation and size/shape of particles also influence the toxicity. Wuttke *et al.* further studied the safety of MIL-100 (Fe), MIL-101 (Cr), and Zr-fumarate nMOFs.[198] Bare or lipid-coated MIL-100 (Fe) and MIL-101 (Cr) were tested on human endothelial cells and lung cells. The nMOFs showed negligible toxicity, except that Fe-containing nMOFs induced cellular stress response on alveolar macrophages. Dental implantation safety of all three nMOFs was also tested. All nMOFs are non-toxic to primary human gingival fibroblasts, whereas only Zr-fumarate nMOF appears to be suitable for coating nerve guidance tubes based on the tests on human primary adult Schwann cells and rat neonatal organotypic DRG cultures.

5. Conclusion

Significant progress has been made in the design of nMOFs for drug delivery, biomedical imaging, and biosensing in the past decade. nMOFs hold distinct advantages over other nanoformulations in biomedical applications due to their intrinsic characteristics that include high porosity, structural tunability/multifunctionality, and biocompatibility. Despite the growing interest and impressive progress in this field, further studies are needed to address several key aspects of nMOFs—controlled synthesis, surface properties, pharmacokinetics and biodistribution, biocompatibility, toxicity, and imaging/therapeutic efficacy— before the biomedical applications of nMOFs can be fully validated to reach the clinical translation stage. We hope that our up-to-date summary and critical assessment of biomedical applications of nMOFs in this review can inspire rigorous interdisciplinary research at the intersection of MOFs and biomedicine to realize the full potential of nMOFs in therapy, biomedical imaging, and biosensing. As the very first nMOF recently entered clinical trial as a radioenhancer for cancer radiotherapy (NCT 03444714), we anticipate a proliferation of nMOFs in clinical testing in the next decade due to the ability to precisely tune nMOF structures and compositions to afford unique functions.

Acknowledgement

We acknowledge the National Cancer Institute (U01-CA198989 and 1R01CA216436), the University of Chicago Medicine Comprehensive Cancer Center (NIH CCSG: P30 CA014599), the Cancer Research Foundation, and the Ludwig Institute for Metastasis Research for funding support.

References

[1]. Eddaoudi M, Kim J, Rosi N, Vodak D, Wachter J, O'Keeffe M, Yaghi OM, Science 2002, 295, 469. [PubMed: 11799235]

[2]. Suh MP, Park HJ, Prasad TK, Lim D-W, Chem. Rev 2011, 112, 782. [PubMed: 22191516]

[3]. Sumida K, Rogow DL, Mason JA, McDonald TM, Bloch ED, Herm ZR, Bae T-H, Long JR, Chem. Rev 2011, 112, 724. [PubMed: 22204561]

[4]. Li J-R, Sculley J, Zhou H-C, Chem. Rev 2011, 112, 869. [PubMed: 21978134]

[5]. He Y, Zhou W, Qian G, Chen B, Chem. Soc. Rev 2014, 43, 5657. [PubMed: 24658531]

[6]. Li J-R, Yu J, Lu W, Sun L-B, Sculley J, Balbuena PB, Zhou H-C, Nat. Comm 2013, 4, 1538.

[7]. Evans OR, Lin W, Acc. Chem. Res 2002, 35, 511. [PubMed: 12118990]

[8]. Wang C, Zhang T, Lin W, Chem. Rev 2011, 112, 1084. [PubMed: 22070202]

[9]. Jain P, Ramachandran V, Clark RJ, Zhou HD, Toby BH, Dalal NS, Kroto HW, Cheetham AK, J. Am. Chem. Soc 2009, 131, 13625. [PubMed: 19725496]

[10]. Zhang W, Xiong R-G, Chem. Rev 2011, 112, 1163. [PubMed: 21939288]

[11]. Ramaswamy P, Wong NE, Shimizu GK, Chem. Soc. Rev 2014, 43, 5913. [PubMed: 24733639]

[12]. Kobayashi Y, Jacobs B, Allendorf MD, Long JR, Chem. Mater 2010, 22, 4120.

[13]. Silva CG, Corma A, García H, J. Mater. Chem 2010, 20, 3141.

[14]. Narayan TC, Miyakai T, Seki S, Dincă M, J. Am. Chem. Soc 2012, 134, 12932. [PubMed: 22827709]

[15]. Talin AA, Centrone A, Ford AC, Foster ME, Stavila V, Haney P, Kinney RA, Szalai V, El Gabaly F, Yoon HP, Science 2014, 343, 66. [PubMed: 24310609]

[16]. Yang F, Xu G, Dou Y, Wang B, Zhang H, Wu H, Zhou W, Li J-R, Chen B, Nat. Energy 2017, 2, 877.

[17]. Kurmoo M, Chem. Soc. Rev 2009, 38, 1353. [PubMed: 19384442]

[18]. Liu J, Chen L, Cui H, Zhang J, Zhang L, Su C-Y, Chem. Soc. Rev 2014, 43, 6011. [PubMed: 24871268]

[19]. Seo JS, Whang D, Lee H, Im Jun S, Oh J, Jeon YJ, Kim K, Nature 2000, 404, 982. [PubMed: 10801124]

[20]. Lee J, Farha OK, Roberts J, Scheidt KA, Nguyen ST, Hupp JT, Chem. Soc. Rev 2009, 38, 1450. [PubMed: 19384447]

[21]. Ma L, Falkowski JM, Abney C, Lin W, Nat. Chem 2010, 2, 838. [PubMed: 20861899]

[22]. Zhao M, Ou S, Wu C-D, Acc. Chem. Res 2014, 47, 1199. [PubMed: 24499017]

[23]. Corma A, García H, Llabrési Xamena F, Chem. Rev 2010, 110, 4606. [PubMed: 20359232]

[24]. Lv X-L, Wang K, Wang B, Su J, Zou X, Xie Y, Li J-R, Zhou H-C, J. Am. Chem. Soc 2017, 139, 211. [PubMed: 27936748]

[25]. Zhang T, Lin W, Chem. Soc. Rev 2014, 43, 5982. [PubMed: 24769551]

[26]. Kent CA, Mehl BP, Ma L, Papanikolas JM, Meyer TJ, Lin W, J. Am. Chem. Soc 2010, 132, 12767. [PubMed: 20735124]

[27]. Wang J-L, Wang C, Lin W, ACS Catal 2012, 2, 2630.

[28]. Hu Z, Deibert BJ, Li J, Chem. Soc. Rev 2014, 43, 5815. [PubMed: 24577142]

[29]. Ma L, Evans OR, Foxman BM, Lin W, Inorg. Chem 1999, 38, 5837.

[30]. Cui Y, Yue Y, Qian G, Chen B, Chem. Rev 2011, 112, 1126. [PubMed: 21688849]

[31]. Allendorf M, Bauer C, Bhakta R, Houk R, Chem. Soc. Rev 2009, 38, 1330. [PubMed: 19384441]

[32]. Allendorf MD, Houk RJ, Andruszkiewicz L, Talin AA, Pikarsky J, Choudhury A, Gall KA, Hesketh PJ, J. Am. Chem. Soc 2008, 130, 14404. [PubMed: 18841964]

[33]. Xie Z, Ma L, deKrafft KE, Jin A, Lin W, J. Am. Chem. Soc 2009, 132, 922.

[34]. Kreno LE, Leong K, Farha OK, Allendorf M, Van Duyne RP, Hupp JT, Chem. Rev 2011, 112, 1105. [PubMed: 22070233]

[35]. Horcajada P, Gref R, Baati T, Allan PK, Maurin G, Couvreur P, Ferey G, Morris RE, Serre C, Chem. Rev 2011, 112, 1232. [PubMed: 22168547]

[36]. Rocca J. Della, Liu D, Lin W, Acc. Chem. Res 2011, 44, 957. [PubMed: 21648429]

[37]. He C, Liu D, Lin W, Chem. Rev 2015, 115, 11079. [PubMed: 26312730]

[38]. Wu MX, Yang YW, Adv. Mater 2017, 29.

[39]. Horcajada P, Serre C, Vallet-Regí M, Sebban M, Taulelle F, Férey G, Angew. chem 2006, 118, 6120.

[40]. Rieter WJ, Taylor KM, An H, Lin W, Lin W, J. Am. Chem. Soc 2006, 128, 9024. [PubMed: 16834362]

[41]. Pelaz B, Alexiou C, Alvarez-Puebla RA, Alves F, Andrews AM, Ashraf S, Balogh LP, Ballerini L, Bestetti A, Brendel C, ACS Publications, 2017.

[42]. Cai W, Chu CC, Liu G, Wáng YXJ, Small 2015, 11, 4806. [PubMed: 26193176]

[43]. Levine DJ, Runčevski T. e., Kapelewski MT, Keitz BK, Oktawiec J, Reed DA, Mason JA, Jiang HZ, Colwell KA, Legendre CM, J. Am. Chem. Soc 2016, 138, 10143. [PubMed: 27486905]

[44]. Teplensky MH, Fantham M, Li P, Wang TC, Mehta JP, Young LJ, Moghadam PZ, Hupp JT, Farha OK, Kaminski CF, J. Am. Chem. Soc 2017.

[45]. Horcajada P, Chalati T, Serre C, Gillet B, Sebrie C, Baati T, Eubank JF, Heurtaux D, Clayette P, Kreuz C, Chang J-S, Hwang YK, Marsaud V, Bories P-N, Cynober L, Gil S, Ferey G, Couvreur P, Gref R, Nat. Mater 2010, 9, 172. [PubMed: 20010827]

[46]. An J, Geib SJ, Rosi NL, J. Am. Chem. Soc 2009, 131, 8376. [PubMed: 19489551]

[47]. An J, Shade CM, Chengelis-Czegan DA, Petoud S, Rosi NL, J. Am. Chem. Soc 2011, 133, 1220. [PubMed: 21204560]

[48]. Tan L-L, Li H, Qiu Y-C, Chen D-X, Wang X, Pan R-Y, Wang Y, Zhang SX-A, Wang B, Yang Y-W, Chem. Sci 2015, 6, 1640. [PubMed: 30154997]

[49]. Tan LL, Li H, Zhou Y, Zhang Y, Feng X, Wang B, Yang YW, Small 2015, 11, 3807. [PubMed: 25919865]

[50]. Tan L-L, Song N, Zhang SX-A, Li H, Wang B, Yang Y-W, J. Mater. Chem. B 2016, 4, 135.

[51]. Wang X-G, Dong Z-Y, Cheng H, Wan S-S, Chen W-H, Zou M-Z, Huo J-W, Deng H-X, Zhang X-Z, Nanoscale 2015, 7, 16061. [PubMed: 26372069]

[52]. Park KS, Ni Z, Côté AP, Choi JY, Huang R, Uribe-Romo FJ, Chae HK, O'Keeffe M, Yaghi OM, Proc. Natl. Acad. Sci. U. S. A 2006, 103, 10186. [PubMed: 16798880]

[53]. Zhuang J, Kuo CH, Chou LY, Liu DY, Weerapana E, Tsung CK, ACS nano 2014, 8, 2812. [PubMed: 24506773]

[54]. Zheng H, Zhang Y, Liu L, Wan W, Guo P, Nyström AM, Zou X, J. Am. Chem. Soc 2016, 138, 962. [PubMed: 26710234]

[55]. Lyu F, Zhang Y, Zare RN, Ge J, Liu Z, Nano Lett 2014, 14, 5761. [PubMed: 25211437]

[56]. Wu X, Ge J, Yang C, Hou M, Liu Z, Chem. Comm 2015, 51, 13408. [PubMed: 26214658]

[57]. Liang K, Ricco R, Doherty CM, Styles MJ, Bell S, Kirby N, Mudie S, Haylock D, Hill AJ, Doonan CJ, Nat. Comm 2015, 6.

[58]. Shieh F-K, Wang S-C, Yen C-I, Wu C-C, Dutta S, Chou L-Y, Morabito JV, Hu P, Hsu M-H, Wu KC-W, J. Am. Chem. Soc 2015, 137, 4276. [PubMed: 25781479]

[59]. Zhang Y, Wang F, Ju E, Liu Z, Chen Z, Ren J, Qu X, Adv. Funct. Mater 2016, 26, 6454.

[60]. Cheng H, Zhu JY, Li SY, Zeng JY, Lei Q, Chen KW, Zhang C, Zhang XZ, Adv. Funct. Mater 2016, 26, 7847.

[61]. Wang J, Li J, Wang Y, Gao M, Zhang X, Yang P, ACS Appl. Mater. Interfaces 2016, 8, 27482. [PubMed: 27681085]

[62]. He L, Wang T, An J, Li X, Zhang L, Li L, Li G, Wu X, Su Z, Wang C, Cryst. Eng. Comm 2014, 16, 3259.

[63]. Li R, Ren X, Zhao J, Feng X, Jiang X, Fan X, Lin Z, Li X, Hu C, Wang B, J. Mater. Chem. A 2014, 2, 2168.

[64]. Bian R, Wang T, Zhang L, Li L, Wang C, Biomater. Sci 2015, 3, 1270. [PubMed: 26236784]

[65]. Pan Y, Liu Y, Zeng G, Zhao L, Lai Z, Chem. Comm 2011, 47, 2071. [PubMed: 21206942]

[66]. Pisklak TJ, Macías M, Coutinho DH, Huang RS, Balkus KJ, Top. Catal 2006, 38, 269.

[67]. Lykourinou V, Chen Y, Wang X-S, Meng L, Hoang T, Ming L-J, Musselman RL, Ma S, J. Am. Chem. Soc 2011, 133, 10382. [PubMed: 21682253]

[68]. Nazari M, Rubio-Martinez M, Tobias G, Barrio JP, Babarao R, Nazari F, Konstas K, Muir BW, Collins SF, Hill AJ, Adv. Funct. Mater 2016, 26, 3244.

[69]. Gadzikwa T, Farha OK, Mulfort KL, Hupp JT, Nguyen ST, Chem. Comm 2009, 3720. [PubMed: 19557260]

[70]. Wang Z, Cohen SM, J. Am. Chem. Soc 2007, 129, 12368. [PubMed: 17880219]

[71]. Costa JS, Gamez P, Black CA, Roubeau O, Teat SJ, Reedijk J, Eur. J. Inorg. Chem 2008, 2008, 1551.

[72]. Britt D, Lee C, Uribe-Romo FJ, Furukawa H, Yaghi OM, Inorg. chem 2010, 49, 6387. [PubMed: 20560600]

[73]. Taylor-Pashow KML, Rocca J. Della, Xie Z, Tran S, Lin W, J. Am. Chem. Soc 2009, 131, 14261. [PubMed: 19807179]

[74]. Morris W, Doonan CJ, Furukawa H, Banerjee R, Yaghi OM, J. Am. Chem. Soc 2008, 130, 12626. [PubMed: 18754585]

[75]. Ingleson MJ, Barrio JP, Guilbaud J-B, Khimyak YZ, Rosseinsky MJ, Chem. Comm 2008, 2680. [PubMed: 18535706]

[76]. Haneda T, Kawano M, Kawamichi T, Fujita M, J. Am. Chem. Soc 2008, 130, 1578. [PubMed: 18189406]

[77]. Burrows AD, Frost CG, Mahon MF, Richardson C, Angew. Chem. Int. Ed 2008, 47, 8482.

[78]. Dugan E, Wang Z, Okamura M, Medina A, Cohen SM, Chem. Comm 2008, 3366. [PubMed: 18633491]

[79]. Volkringer C, Cohen SM, Angew. Chem. Int. Ed 2010, 49, 4644.

[80]. He C, Lu K, Lin W, J. Am. Chem. Soc 2014, 136, 12253. [PubMed: 25136764]

[81]. Goto Y, Sato H, Shinkai S, Sada K, J. Am. Chem. Soc 2008, 130, 14354. [PubMed: 18839949]

[82]. Liu C, Li T, Rosi NL, J. Am. Chem. Soc 2012, 134, 18886. [PubMed: 23113571]

[83]. Custelcean R, Gorbunova MG, J. Am. Chem. Soc 2005, 127, 16362. [PubMed: 16305200]
[84]. Carboni M, Lin Z, Abney CW, Zhang T, Lin W, Chem. - Eur. J 2014, 20, 14965. [PubMed: 25294005]
[85]. Carboni M, Abney CW, Liu S, Lin W, Chem. Sci 2013, 4, 2396.
[86]. Diring S, Wang DO, Kim C, Kondo M, Chen Y, Kitagawa S, Kamei K.-i., Furukawa S, Nat. Comm 2013, 4, 2684.
[87]. Morris W, Briley WE, Auyeung E, Cabezas MD, Mirkin CA, J. Am. Chem. Soc 2014.
[88]. Chen WH, Yu X, Liao WC, Sohn YS, Cecconello A, Kozell A, Nechushtai R, Willner I, Adv. Funct. Mater 2017.
[89]. He C, Lu K, Liu D, Lin W, J. Am. Chem. Soc 2014, 136, 5181. [PubMed: 24669930]
[90]. Liu J, Zhang L, Lei J, Shen H, Ju H, ACS Appl. Mater. Interfaces 2017, 9, 2150. [PubMed: 28033467]
[91]. Xu R, Wang Y, Duan X, Lu K, Micheroni D, Hu A, Lin W, J. Am. Chem. Soc 2016, 138, 2158. [PubMed: 26864385]
[92]. Diring S, Carné-Sánchez A, Zhang J, Ikemura S, Kim C, Inaba H, Kitagawa S, Furukawa S, Chem. Sci 2017, 8, 2381. [PubMed: 28451343]
[93]. Wang C, Xie Z, Lin W, J. Am. Chem. Soc 2011, 133, 13445. [PubMed: 21780787]
[94]. Kim C, Diring S, Furukawa S, Kitagawa S, Dalton Trans 2015, 44, 15324. [PubMed: 26226560]
[95]. Nguyen JG, Tanabe KK, Cohen SM, Cryst. Eng. Comm 2010, 12, 2335.
[96]. Martí-Gastaldo C, Warren JE, Stylianou KC, Flack NL, Rosseinsky MJ, Angew. Chem. Int. Ed 2012, 51, 11044.
[97]. Katsoulidis AP, Park KS, Antypov D, Martí-Gastaldo C, Miller GJ, Warren JE, Robertson CM, Blanc F, Darling GR, Berry NG, Angew. Chem. Int. Ed 2014, 53, 193.
[98]. Martí-Gastaldo C, Antypov D, Warren J, Briggs M, Chater PA, Wiper PV, Miller GJ, Khimyak Y, Darling GR, Berry NG, Nat. Chem 2014, 6, 343. [PubMed: 24651203]
[99]. Mantion A, Massüger L, Rabu P, Palivan C, McCusker LB, Taubert A, J. Am. Chem. Soc 2008, 130, 2517. [PubMed: 18247607]
[100]. Rieter WJ, Pott KM, Taylor KML, Lin W, J. Am. Chem. Soc 2008, 130, 11584. [PubMed: 18686947]
[101]. Huxford-Phillips RC, Russell SR, Liu D, Lin W, RSC Adv 2013, 3, 14438. [PubMed: 24058727]
[102]. Liu D, Poon C, Lu K, He C, Lin W, Nat. Comm 2014, 5, 4182.
[103]. He C, Liu D, Lin W, ACS nano 2015, 9, 991. [PubMed: 25559017]
[104]. He C, Liu D, Lin W, Biomaterials 2015, 36, 124. [PubMed: 25315138]
[105]. Poon C, He C, Liu D, Lu K, Lin W, J. Controlled Release 2015, 201, 90.
[106]. He C, Poon C, Chan C, Yamada SD, Lin W, J. Am. Chem. Soc 2016, 138, 6010. [PubMed: 27088560]
[107]. He C, Duan X, Guo N, Chan C, Poon C, Weichselbaum RR, Lin W, Nat. Comm 2016, 7.
[108]. Lu K, He C, Lin W, J. Am. Chem. Soc 2014, 136, 16712. [PubMed: 25407895]
[109]. Dai R, Peng F, Ji P, Lu K, Wang C, Sun J, Lin W, Inorganic Chemistry 2017.
[110]. Cliffe MJ, Castillo-Martínez E, Wu Y, Lee J, Forse AC, Firth FC, Moghadam PZ, Fairen-Jimenez D, Gaultois MW, Hill JA, Journal of the American Chemical Society 2017.
[111]. Lan G, Ni K, Lin W, Coord. Chem. Rev 2017.
[112]. Lovell JF, Jin CS, Huynh E, Jin H, Kim C, Rubinstein JL, Chan WC, Cao W, Wang LV, Zheng G, Nat. Mater 2011, 10, 324. [PubMed: 21423187]
[113]. Yoon HK, Lou X, Chen Y-C, Koo Lee Y-E, Yoon E, Kopelman R, Chem. Mater 2014, 26, 1592. [PubMed: 24701030]
[114]. Liu K, Xing R, Zou Q, Ma G, Möhwald H, Yan X, Angew. Chem. Int. Ed 2016, 55, 3036.
[115]. Zhang N, Zhao F, Zou Q, Li Y, Ma G, Yan X, Small 2016, 12, 5936. [PubMed: 27622681]
[116]. Yang X, Fei J, Li Q, Li J, Chem. - Eur. J 2016, 22, 6477. [PubMed: 26934079]
[117]. Lu K, He C, Lin W, J. Am. Chem. Soc 2015, 137, 7600. [PubMed: 26068094]

[118]. Lu K, He C, Guo N, Chan C, Ni K, Weichselbaum RR, Lin W, J. Am. Chem. Soc 2016, 138, 12502. [PubMed: 27575718]

[119]. Smith DM, Simon JK, Baker JR Jr, Nat. Rev. Immunol 2013, 13, 592. [PubMed: 23883969]

[120]. Lismont M, Dreesen L, Wuttke S, Adv. Funct. Mater 2017, 27.

[121]. Liu J, Yang Y, Zhu W, Yi X, Dong Z, Xu X, Chen M, Yang K, Lu G, Jiang L, Biomaterials 2016, 97, 1. [PubMed: 27155362]

[122]. Park J, Jiang Q, Feng D, Mao L, Zhou H-C, J. Am. Chem. Soc 2016, 138, 3518. [PubMed: 26894555]

[123]. Li S-Y, Cheng H, Xie B-R, Qiu W-X, Zeng J-Y, Li C-X, Wan S-S, Zhang L, Liu W, Zhang X, ACS nano 2017.

[124]. Murray LJ, Dincă M, Long JR, Chem. Soc. Rev 2009, 38, 1294. [PubMed: 19384439]

[125]. Chughtai AH, Ahmad N, Younus HA, Laypkov A, Verpoort F, Chem. Soc. Rev 2015, 44, 6804. [PubMed: 25958955]

[126]. Manna K, Ji P, Lin Z, Greene FX, Urban A, Thacker NC, Lin W, Nat. Comm 2016, 7.

[127]. Wyszogrodzka G, Marszałek B, Gil B, Dorożyński P, Drug discovery today 2016, 21, 1009. [PubMed: 27091434]

[128]. Chen D, Yang D, Dougherty CA, Lu W, Wu H, He X, Cai T, Van Dort ME, Ross BD, Hong H, ACS nano 2017, 11, 4315. [PubMed: 28345871]

[129]. Chen D, Yang D, Lu W, Hong H, J. Nucl. Med 2017, 58, 129. [PubMed: 27469356]

[130]. Wheatley PS, Butler AR, Crane MS, Fox S, Xiao B, Rossi AG, Megson IL, Morris RE, J. Am. Chem. Soc 2006, 128, 502. [PubMed: 16402837]

[131]. Xiao B, Wheatley PS, Zhao X, Fletcher AJ, Fox S, Rossi AG, Megson IL, Bordiga S, Regli L, Thomas KM, Morris RE, J. Am. Chem. Soc 2007, 129, 1203. [PubMed: 17263402]

[132]. Ingleson MJ, Heck R, Gould JA, Rosseinsky MJ, Inorg. chem 2009, 48, 9986. [PubMed: 19795833]

[133]. Ma M, Noei H, Mienert B, Niesel J, Bill E, Muhler M, Fischer RA, Wang Y, Schatzschneider U, Metzler-Nolte N, Chem. - Eur. J 2013, 19, 6785. [PubMed: 23536364]

[134]. Chen Q, Xu M, Zheng W, Xu T, Deng H, Liu J, ACS Appl. Mater. Interfaces 2017, 9, 6712. [PubMed: 28191840]

[135]. Wang S, McGuirk CM, Ross MB, Wang S, Chen P, Xing H, Liu Y, Mirkin CA, J. Am. Chem. Soc 2017.

[136]. Wang W, Wang L, Li Z, Xie Z, Chem. Comm 2016, 52, 5402. [PubMed: 27009757]

[137]. Lázaro IA, Haddad S, Sacca S, Orellana-Tavra C, Fairen-Jimenez D, Forgan RS, Chem 2017, 2, 561. [PubMed: 28516168]

[138]. Sontz PA, Bailey JB, Ahn S, Tezcan FA, J. Am. Chem. Soc 2015, 137, 11598. [PubMed: 26305584]

[139]. Bailey JB, Zhang L, Chiong JA, Ahn S, Tezcan FA, J. Am. Chem. Soc 2017.

[140]. Khoo VS, Dearnaley DP, Finnigan DJ, Padhani A, Tanner SF, Leach MO, Radiotherapy and oncology : journal of the European Society for Therapeutic Radiology and Oncology 1997, 42, 1. [PubMed: 9132820]

[141]. Ersoy H, Rybicki FJ, J. Magn. Reson. Imaging 2007, 26, 1190. [PubMed: 17969161]

[142]. Caravan P, Chem. Soc. Rev 2006, 35, 512. [PubMed: 16729145]

[143]. Wu MX, Yang YW, Advanced Materials 2017.

[144]. Rieter WJ, Taylor KM, An H, Lin W, Lin W, Journal of the American Chemical Society 2006, 128, 9024. [PubMed: 16834362]

[145]. Taylor KM, Jin A, Lin W, Angew. Chem. Int. Ed 2008, 47, 7722.

[146]. Taylor KM, Rieter WJ, Lin W, J. Am. Chem. Soc 2008, 130, 14358. [PubMed: 18844356]

[147]. Caravan P, Ellison JJ, McMurry TJ, Lauffer RB, Chem. Rev 1999, 99, 2293. [PubMed: 11749483]

[148]. Yang Y, Liu J, Liang C, Feng L, Fu T, Dong Z, Chao Y, Li Y, Lu G, Chen M, Liu Z, ACS nano 2016, 10, 2774. [PubMed: 26799993]

[149]. Ray Chowdhuri A, Bhattacharya D, Sahu SK, Dalton Trans 2016, 45, 2963. [PubMed: 26754449]

[150]. Gao X, Zhai M, Guan W, Liu J, Liu Z, Damirin A, ACS Appl. Mater. Interfaces 2017, 9, 3455. [PubMed: 28079361]

[151]. Zhang Y, Liu C, Wang F, Liu Z, Ren J, Qu X, Chem. Comm 2017, 53, 1840. [PubMed: 28111662]

[152]. Paulus MJ, Gleason SS, Easterly ME, Foltz CJ, Lab animal 2001, 30, 36.

[153]. Brenner DJ, Hall EJ, Engl N J. Med 2007, 357, 2277.

[154]. Dekrafft KE, Boyle WS, Burk LM, Zhou OZ, Lin W, J. Mater. Chem 2012, 22, 18139. [PubMed: 23049169]

[155]. Zhang T, Wang L, Ma C, Wang W, Ding J, Liu S, Zhang X, Xie Z, J. Mater. Chem. B 2017, 5, 2330.

[156]. Shang W, Zeng C, Du Y, Hui H, Liang X, Chi C, Wang K, Wang Z, Tian J, Adv. Mater 2017, 29.

[157]. Foucault-Collet A, Gogick KA, White KA, Villette S, Pallier A, Collet G, Kieda C, Li T, Geib SJ, Rosi NL, Petoud S, Proc. Natl. Acad. Sci. U. S. A 2013, 110, 17199. [PubMed: 24108356]

[158]. Li Y, Tang J, He L, Liu Y, Liu Y, Chen C, Tang Z, Adv. Mater 2015, 27, 4075. [PubMed: 26053933]

[159]. Cai W, Gao H, Chu C, Wang X, Wang J, Zhang P, Lin G, Li W, Liu G, Chen X, ACS Appl. Mater. Interfaces 2017, 9, 2040. [PubMed: 28032505]

[160]. Liu W, Wang YM, Li YH, Cai SJ, Yin XB, He XW, Zhang YK, small 2017, 13.

[161]. Asgharzadeh MR, Barar J, Pourseif MM, Eskandani M, Niya M. Jafari, Mashayekhi MR, Omidi Y, BioImpacts : BI 2017, 7, 115. [PubMed: 28752076]

[162]. Wu P, Wang J, He C, Zhang X, Wang Y, Liu T, Duan C, Adv. Funct. Mater 2012, 22, 1698.

[163]. Ma Y, Su H, Kuang X, Li X, Zhang T, Tang B, Anal. Chem 2014, 86, 11459. [PubMed: 25342497]

[164]. Nagarkar SS, Saha T, Desai AV, Talukdar P, Ghosh SK, Sci. Rep 2014, 4.

[165]. Nagarkar SS, Desai AV, Ghosh SK, Chem. - Eur. J 2015, 21, 9994. [PubMed: 26096215]

[166]. Zhang X, Hu Q, Xia T, Zhang J, Yang Y, Cui Y, Chen B, Qian G, ACS Appl. Mater. Interfaces 2016, 8, 32259. [PubMed: 27933828]

[167]. Lu Y, Yan B, Liu JL, Chem. Comm 2014, 50, 9969. [PubMed: 25034974]

[168]. Zhou Y, Chen H-H, Yan B, J. Mater. Chem. A 2014, 2, 13691.

[169]. Zhao J, Wang Y-N, Dong W-W, Wu Y-P, Li D-S, Zhang Q-C, Inorg. Chem 2016, 55, 3265. [PubMed: 26967044]

[170]. Yang C-X, Ren H-B, Yan X-P, Anal. Chem 2013, 85, 7441. [PubMed: 23826852]

[171]. Wang B, Yang Q, Guo C, Sun Y, Xie L-H, Li J-R, ACS Appl. Mater. Interfaces 2017, 9, 10286. [PubMed: 28248079]

[172]. Hornung V, Latz E, Nat. Rev. Immunol 2010, 10, 123. [PubMed: 20098460]

[173]. Chen L, Zheng H, Zhu X, Lin Z, Guo L, Qiu B, Chen G, Chen Z-N, Analyst 2013, 138, 3490. [PubMed: 23665537]

[174]. Fangguo J, Meili C, Lihu X, Zhihuang C, Fangli Y, RSC Adv 2014, 4, 9379.

[175]. Zhang H-T, Zhang J-W, Huang G, Du Z-Y, Jiang H-L, Chem. Comm 2014, 50, 12069. [PubMed: 25164253]

[176]. Ye T, Liu Y, Luo M, Xiang X, Ji X, Zhou G, He Z, Analyst 2014, 139, 1721. [PubMed: 24524118]

[177]. Wu Y, Han J, Xue P, Xu R, Kang Y, Nanoscale 2015, 7, 1753. [PubMed: 25514895]

[178]. Mejia-Ariza R, Rosselli J, Breukers C, Manicardi A, Terstappen LW, Corradini R, Huskens J, Chem. - Eur. J 2017, 23, 4180. [PubMed: 28139850]

[179]. Zhao D, Zhang J, Yue D, Lian X, Cui Y, Yang Y, Qian G, Chem. Comm 2016, 52, 8259. [PubMed: 27284589]

[180]. Giménez-Marqués M, Hidalgo T, Serre C, Horcajada P, Coord. Chem. Rev 2016, 307, 342.

[181]. Carné-Sánchez A, Imaz I, Cano-Sarabia M, Maspoch D, Nat. Chem 2013, 5, 203. [PubMed: 23422562]

[182]. Kundu T, Mitra S, Patra P, Goswami A, Díaz Díaz D, Banerjee R, Chem. - Eur. J 2014, 20, 10514. [PubMed: 25044210]

[183]. Albanese A, Tang PS, Chan WC, Annu. Rev. Biomed. Eng 2012, 14, 1. [PubMed: 22524388]

[184]. Choi HS, Liu W, Misra P, Tanaka E, Zimmer JP, Ipe BI, Bawendi MG, Frangioni JV, Nat. biotech 2007, 25, 1165.

[185]. Moghimi SM, Hunter AC, Murray JC, Pharmacol. Rev 2001, 53, 283. [PubMed: 11356986]

[186]. Jiang W, Kim BY, Rutka JT, Chan WC, Nat. nanotech 2008, 3, 145.

[187]. Chithrani BD, Ghazani AA, Chan WC, Nano lett 2006, 6, 662. [PubMed: 16608261]

[188]. Rieter WJ, Taylor KM, Lin W, J. Am. Chem. Soc 2007, 129, 9852. [PubMed: 17645339]

[189]. Agostoni V, Horcajada P, Noiray M, Malanga M, Aykaç A, Jicsinszky L, Vargas-Berenguel A, Semiramoth N, Daoud-Mahammed S, Nicolas V, Sci. Rep 2015, 5.

[190]. Meng X, Gui B, Yuan D, Zeller M, Wang C, Sci. Adv 2016, 2, e1600480. [PubMed: 27493996]

[191]. Bellido E, Hidalgo T, Lozano MV, Guillevic M, Simón-Vázquez R, Santander-Ortega MJ, González-Fernández Á, Serre C, Alonso MJ, Horcajada P, Adv. Healthcare Mater 2015, 4, 1246.

[192]. Rowe MD, Chang C-C, Thamm DH, Kraft SL, Harmon JF Jr, Vogt AP, Sumerlin BS, Boyes SG, Langmuir 2009, 25, 9487. [PubMed: 19422256]

[193]. Rowe MD, Thamm DH, Kraft SL, Boyes SG, Biomacromolecules 2009, 10, 983. [PubMed: 19290624]

[194]. Deng K, Hou Z, Li X, Li C, Zhang Y, Deng X, Cheng Z, Lin J, Sci. Rep 2015, 5.

[195]. Wilhelm S, Tavares AJ, Dai Q, Ohta S, Audet J, Dvorak HF, Chan WC, Nat. Rev. Mater 2016, 1, 16014.

[196]. Baati T, Njim L, Neffati F, Kerkeni A, Bouttemi M, Gref R, Najjar MF, Zakhama A, Couvreur P, Serre C, Chem. Sci 2013, 4, 1597.

[197]. Ruyra À, Yazdi A, Espín J, Carné-Sánchez A, Roher N, Lorenzo J, Imaz I, Maspoch D, Chem. - Eur. J 2015, 21, 2508. [PubMed: 25504892]

[198]. Wuttke S, Zimpel A, Bein T, Braig S, Stoiber K, Vollmar A, Müller D, Haastert-Talini K, Schaeske J, Stiesch M, Adv. Healthcare Mater 2017, 6.

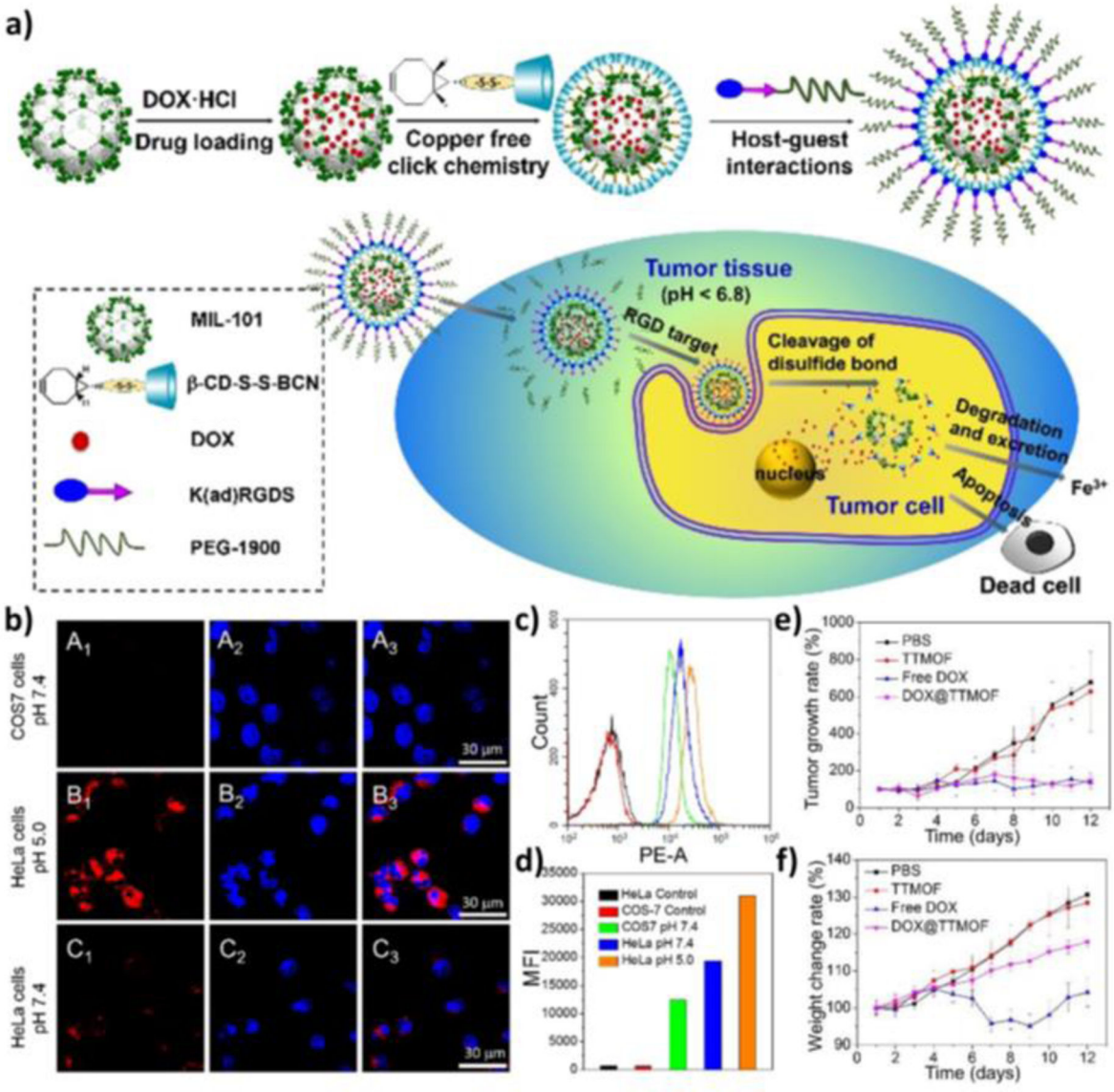

Figure 1.

(a) Schematic illustration of the MIL-101(Fe) nMOF design, its targeted delivery, and anticancer process. (b) Confocal images showing tumor-specific cellular uptake of DOX@TTMOF at different pH. Dot plots (c) and mean fluorescence intensity (d) of quantitative flow cytometry analysis. Tumor volume (e) and body weight (f) changes in H-22 tumor-bearing mice after treatment. Reproduced with permission.[51] Copyright 2015 The Royal Society of Chemistry.

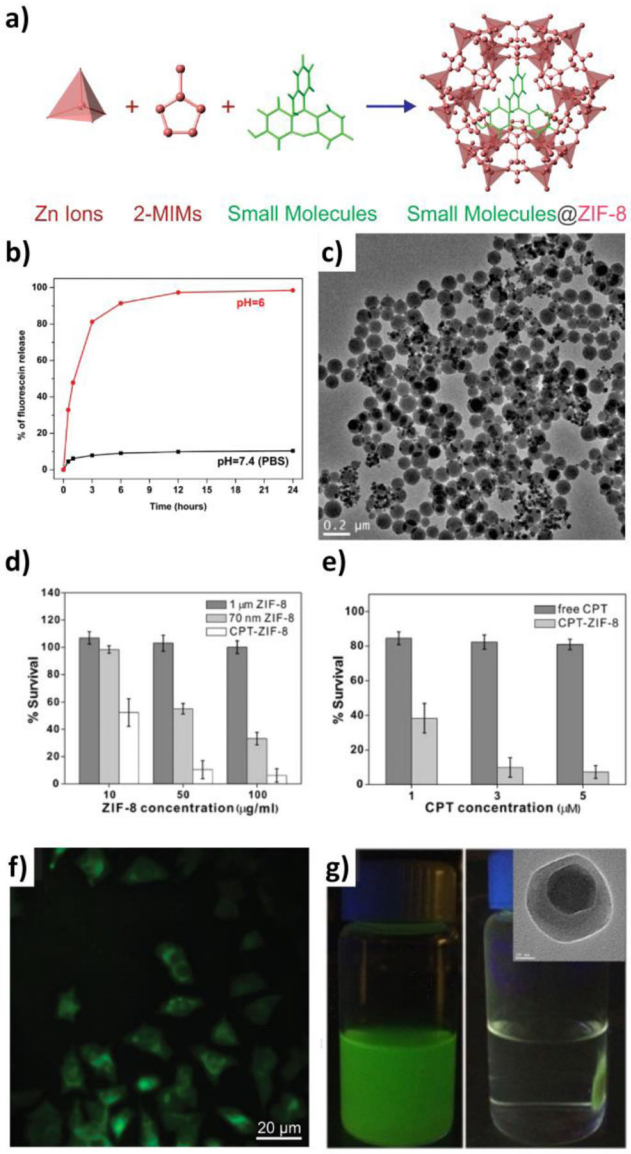

Figure 2.

(a) Scheme showing the encapsulation of small molecules into ZIF-8 during nMOF growth. (b) Fluorescein release profiles in PBS (black squares) and pH 6.0 buffer solution (red circles). (c) TEM image of fluorescein-encapsulated nanospheres dispersed in PBS for one day. (d) Cell viability when incubated with micron-sized ZIF-8 (dark gray), 70 nm ZIF-8 (light gray), and CPT encapsulated ZIF-8 (white). (e) Cell viability when incubated with free CPT (dark gray), and CPT-encapsulated ZIF-8 (light gray) for 24 h. (f) Fluorescence microscopy images of cells incubated with 70 nm fluorescein-encapsulated ZIF-8. (g) Fe_3O_4@ZIF-8 nanospheres migrated to sides of a vial upon application of an external magnetic field; inset: TEM image of single Fe_3O_4@ZIF-8 nanosphere. Reproduced with permission.[53] Copyright 2014, American Chemical Society.

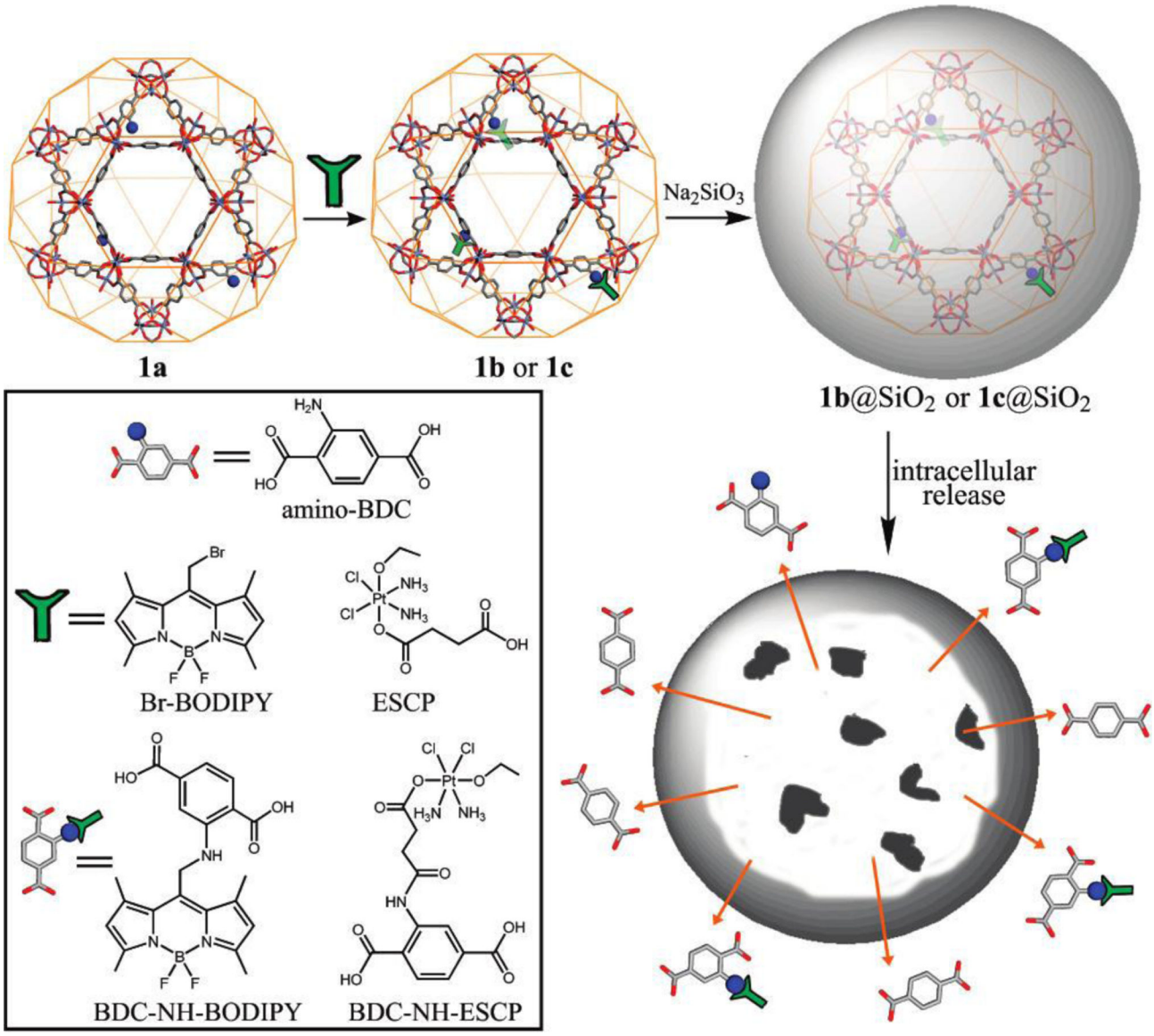

Figure 3.

Schematic representation of the drug attachment and surface modification of Fe(III)-MIL-101 nMOFs. Reproduced with permission.[73] Copyright 2009, American Chemical Society.

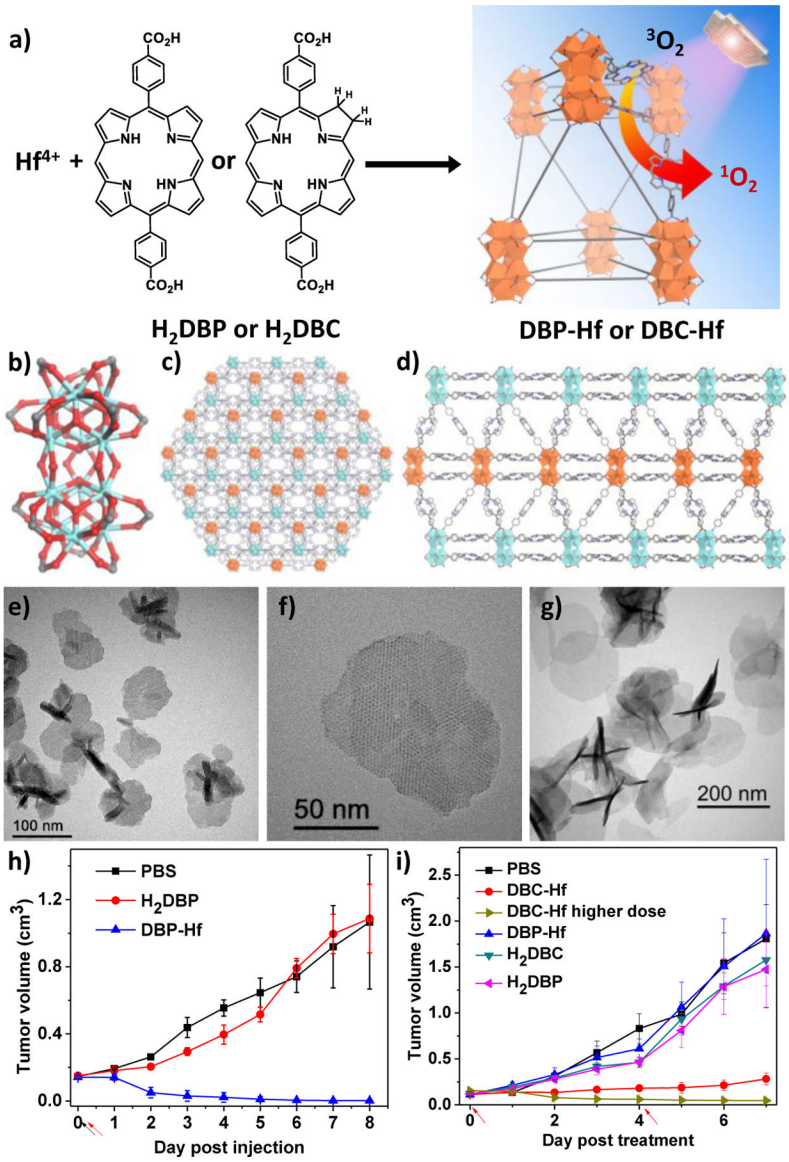

Figure 4.

(a) Schematic description of the synthesis of DBP-Hf or DBC-Hf and the singlet oxygen generation process. The structure of Hf_{12} SBU (b) and the idealized crystal structure of DBP-Hf viewed along the *c* axis (c) and the *a* axis (d). TEM (e) and high-resolution TEM (f) images of DBP-Hf showing nanoplate morphology. (g) TEM image of DBC-Hf. *In vivo* tumor regression after PDT treatment of DBP-Hf (h) and DBC-Hf (i) on different tumor-bearing mice models, along with the control groups. Black and red arrows refer to the time of injection and irradiation, respectively. Reproduced with permission.[108, 117] Copyright 2014 and 2015, American Chemical Society.

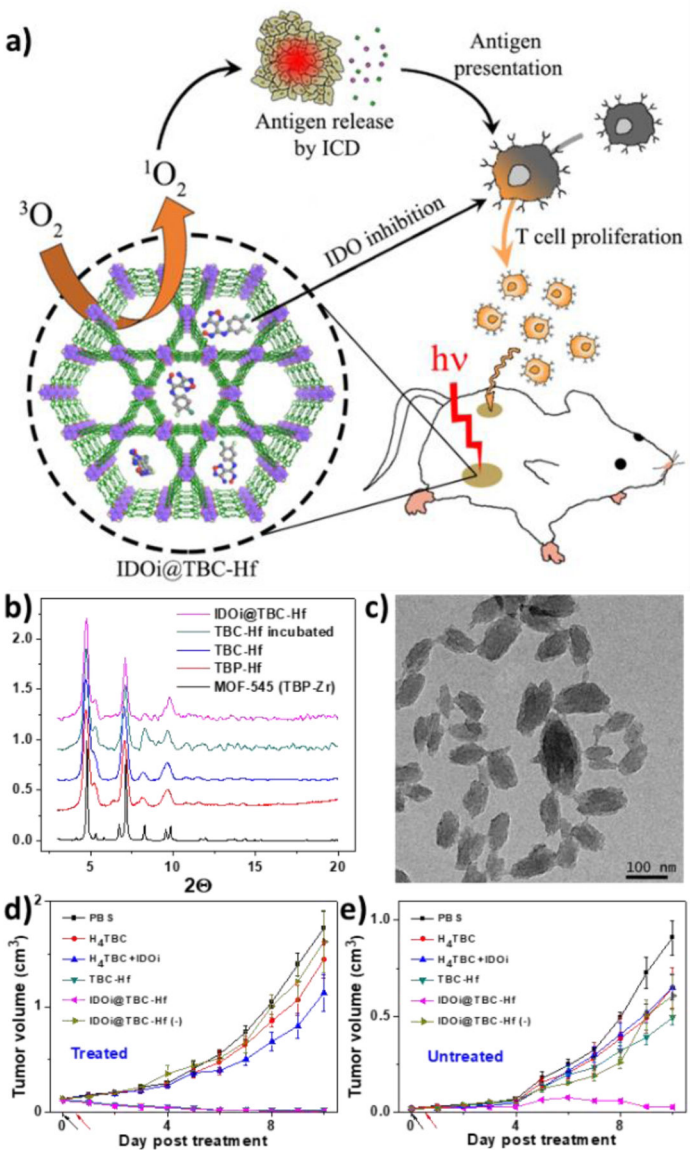

Figure 5.

(a) Schematic presentation of combined PDT and immunotherapy by IDOi@TBC-Hf. PXRD (b) and TEM image (c) of the nMOFs. *In vivo* anticancer efficacy of PDT treated (d) and untreated (e) tumors showing that IDOi@TBC-Hf enabled PDT induced abscopal effects. Reproduced with permission.[118] Copyright 2016, American Chemical Society.

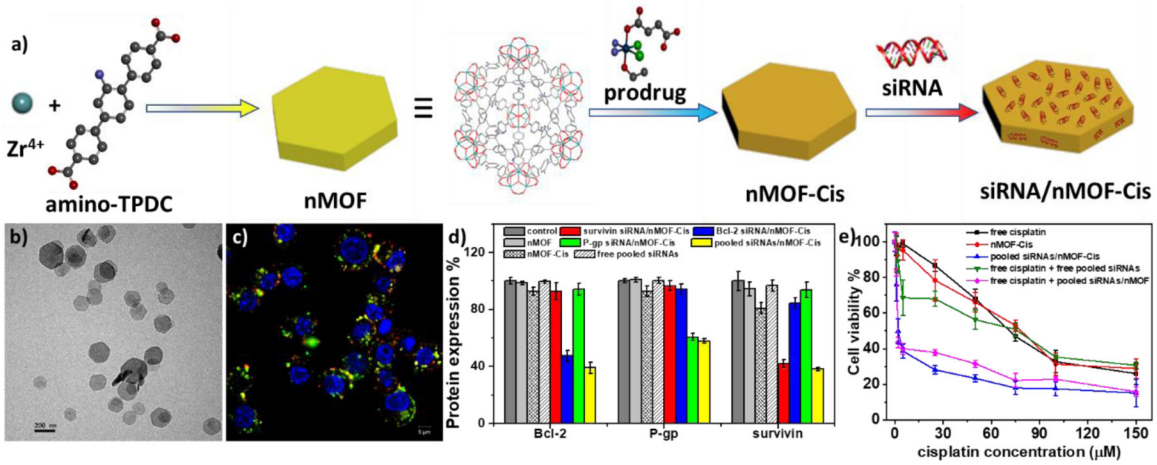

Figure 6.

(a) Schematic presentation of siRNA/nMOF-Cis synthesis and drug loading. (b) TEM image of siRNA/nMOF-Cis nanoparticles. (c) Confocal microscopy image showing siRNA endosomal escape. (d) Gene silencing efficiency of siRNA/nMOF-Cis expressed as percentage of protein expression. (e) In vitro anticancer efficacy on SKOV-3 cells showing re-sensitization effect with siRNA/nMOF-Cis. Reproduced with permission.[89] Copyright 2014, American Chemical Society.

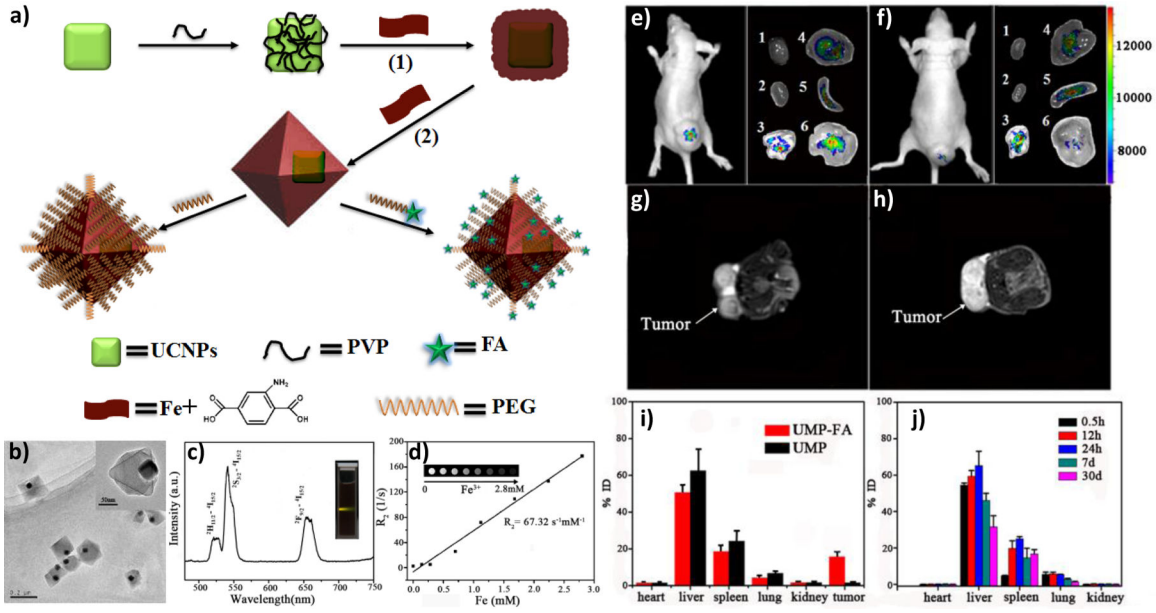

Figure 7.

(a) Scheme showing the synthesis and functionalization of UCNP@Fe-MIL-101_NH_2 nanostructures. (b) TEM image of UMPs nanoparticles with core-shell structure. (c) Upconversion emission spectra of UMP nanostructures. Inset is the photo of UMPs nanostructures dispersed in water under 980 nm diode excitation. (d) Relaxation rate R_2 ($1/T_2$) versus molar concentrations of UMPs nanostructures at room temperature using a 3T MRI scanner (Inset: T_2-weighted MR images of UMPs with varied concentrations). Representative upconversion luminescence (e,f) and T_2-MRI images (g,h) of subcutaneous KB tumor-bearing mice (tumor diameter: 8–10 mm) and dissected organs of the mice sacrificed 24 h after intravenous injection of UMP-FAs (targeted, e,g) and UMPs (non-targeted, f,h). 1, heart; 2, kidney; 3, lung; 4, liver; 5, spleen; 6, KB tumor. (i) Biodistribution of nanostructures in organs of the tumor-bearing mice 24h after intravenous injection of particles. (j) Biodistribution of intravenously injected UMPs nanostructures in different organs of mice at 0.5 h, 12 h, 24 h, 7 d, and 30 d. Reproduced with permission.[158] Copyright 2015, Wiley-VCH.

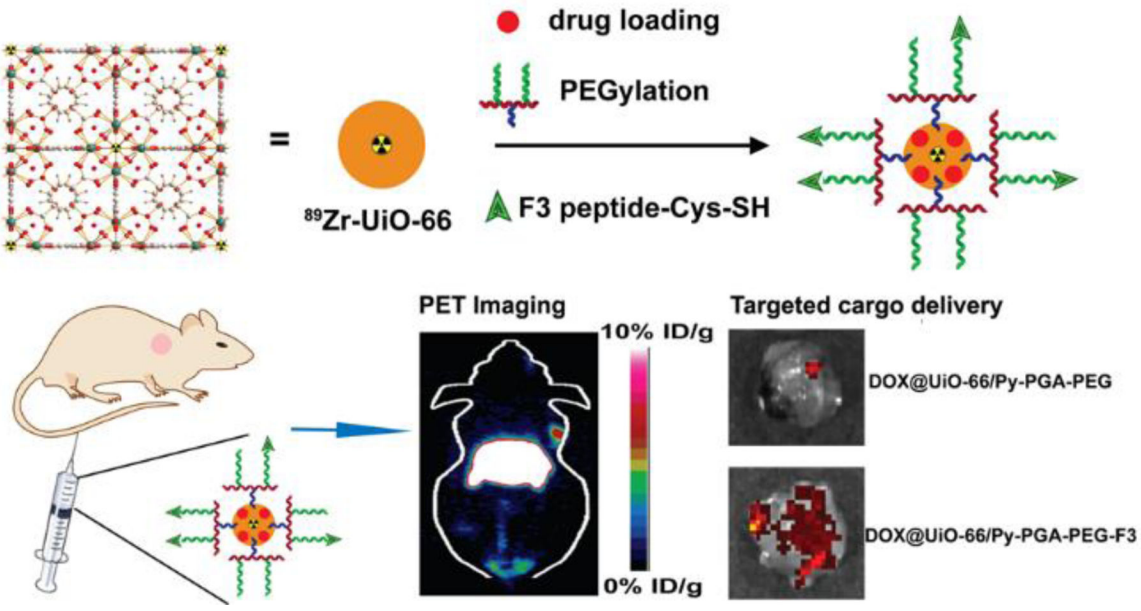

Figure 8.

Schematic illustration of the ^{89}Zr-UiO-66 nMOF formulation and its use in PET imaging and drug delivery. Reproduced with permission.[128] Copyright 2017, American Chemical Society.

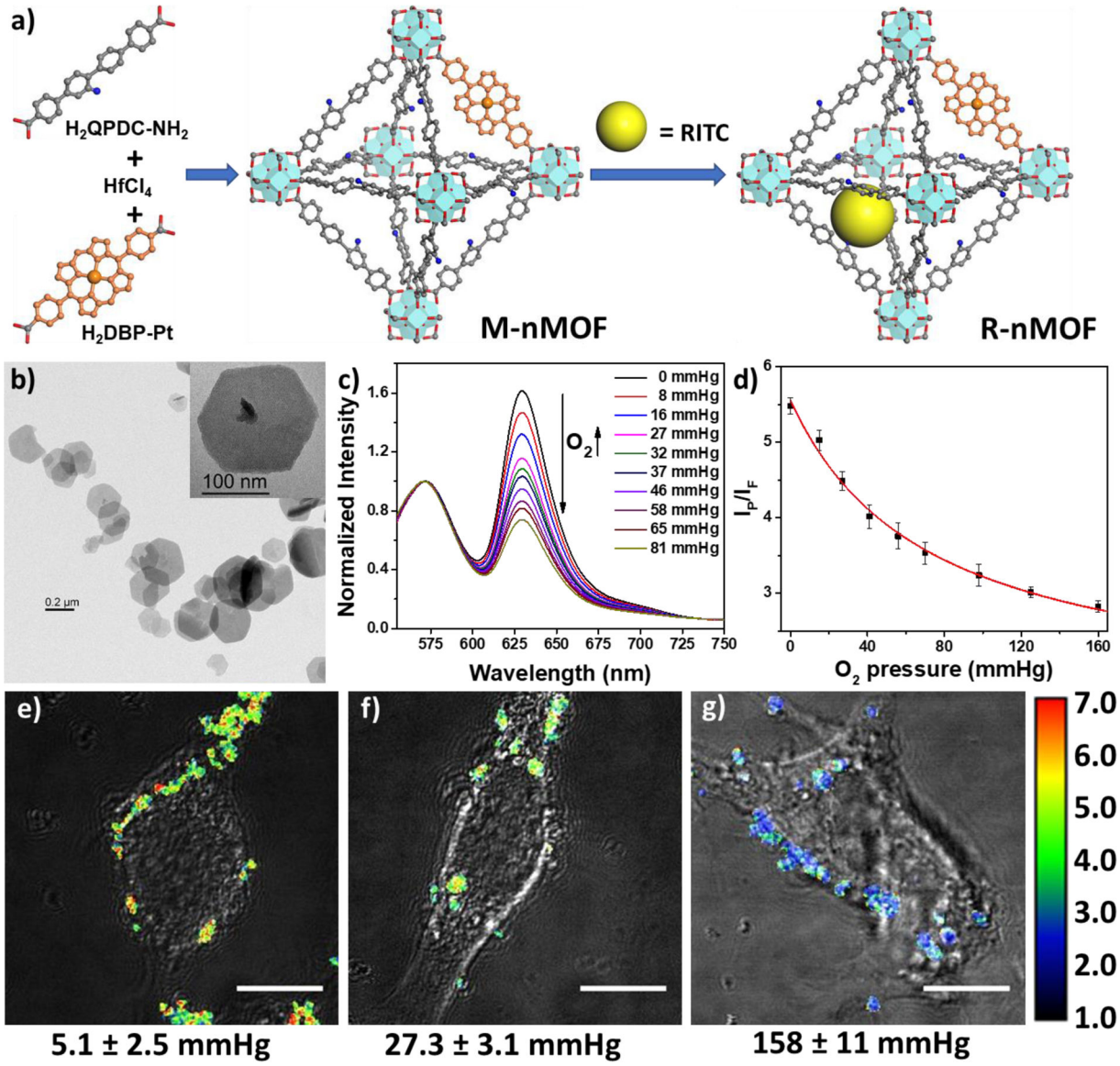

Figure 9.

(a) Scheme showing the nMOF synthesis and fluorophore attachment of R-nMOF. (b) TEM image of R-nMOF. (c) Emission spectra of R-nMOF in HBSS buffer under various oxygen partial pressures with excitation wavelength at 514 nm. (d) Calibration curve of the phosphorescence/fluorescence intensity of R-nMOF on CLSM under different oxygen partial pressures. Ratiometric luminescence imaging (λ_{ex}=514 nm) of CT26 cells after incubation with R-nMOF under hypoxia (e), normoxia (f), and aerated (g) conditions. Scale bar: 10 μm. Reproduced with permission.[91] Copyright 2016, American Chemical Society.

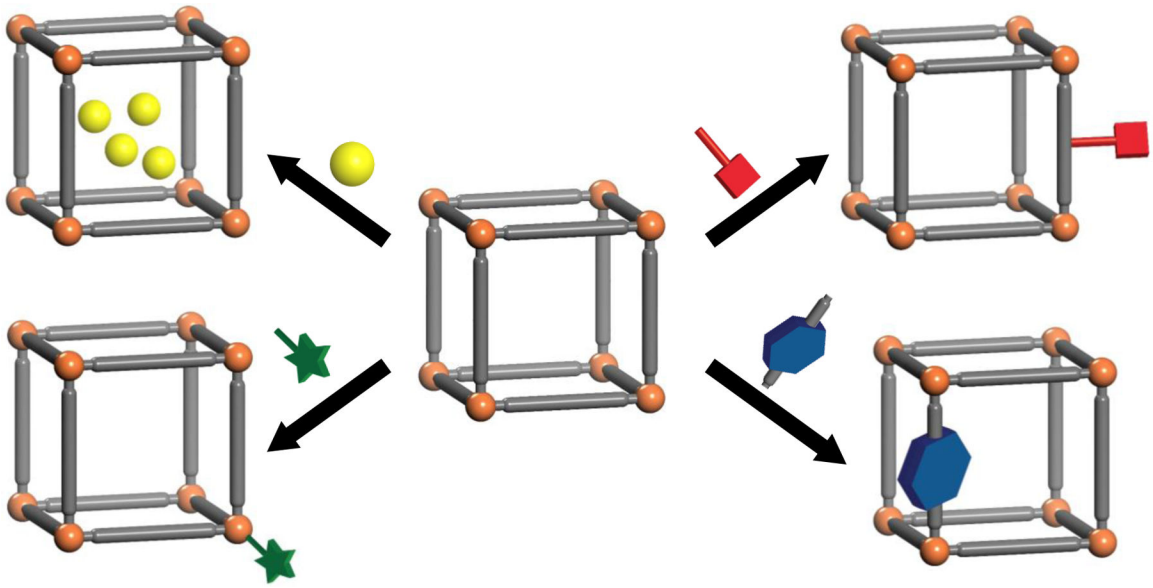

Scheme 1.

Four common strategies for loading drugs into nMOFs (shown clockwise from top left): noncovalent encapsulation, conjugation to the linkers, use of therapeutics as linkers, and attachment to the SBUs.

Table 1.

Stability after culture medium incubation and toxicity of nMOFs.

MOF type	Deg_{min} %[a]	PXRD	*In vitro* toxicity	*In vivo* toxicity
UiO-66	1.8±0.2	stable	+	1
UiO-66-NH_2	2.6±0.3	stable	++	ND
UiO-67	0.3±0.0	amorphous	+	1
Fe-MIL-100	1.1±0.2	stable	++	2
Fe-MIL-101	1.1±0.3	amorphous	++	3
ZIF-7	4.5±0.2	stable	++	2
ZIF-8	19.1±0.8	stable	+++	3
MOF-5	7.8±1.6	new crystalline species	+++	ND
HKUST-1	30.3±0.5	loss of crystallinity	++++	4
NOTT-100	39.4±0.8	loss of crystallinity	+++	ND
Co-MOF-74	16.2±0.3	loss of crystallinity	+	1
Ni-MOF-74	35.1±0.9	stable	+	ND
Mg-MOF-74	62.9±1.4	loss of crystallinity	+	0
Mn-MOF-74	13.3±0.4	loss of crystallinity	++++	ND
Zn-MOF-74	27.2±0.5	stable	+++	ND
Cu-MOF-74	47.9±3.4	loss of crystallinity	++++	ND

[a] The minimum percentage of degradation (Deg_{min} %) was calculated from the metal content in the culture medium solution versus the total amount in the initial MOFs.